CLS
COLLECTE LOCALISATION SATELLITES

Consortium Members

TU Delft Delft University of Technology | SATOC Satellite Oceanographic Consultants | DTU Space National Space Institute | isardSAT | National Oceanography Centre Natural Environment Research Council | NOVELTIS | Starlab Living Science | U.PORTO Faculdade de Ciências Universidade do Porto

ESA Cryosat Plus for Oceans

Validation Report: WP5000 Assessment of SAMOSA SAR solution (ESRIN)

Reference:	CLS-DOS-NT-14-084
Nomenclature:	CP4O-WP5000-VR-04
Issue:	1. 0
Date:	May. 20, 14

esa European Space Agency

cnes CENTRE NATIONAL D'ÉTUDES SPATIALES

Chronology Issues:			
Issue:	Date:	Reason for change:	Author
1.0	20/05/14	Creation of Issue 1.0 document	M. Raynal T. Moreau

People involved in this issue:		
Written by (*):	M. Raynal (CLS) T. Moreau (CLS)	Date + Initials:(visa or ref)
Checked by (*):	S. Labroue (CLS)	Date + Initial:(visa ou ref)
Approved by (*):	F. Boy (CNES)	Date + Initial:(visa ou ref)
Application authorized by (*):	(ESA) N. Picot (CNES)	Date + Initial:(visa ou ref)

**In the opposite box: Last and First name of the person + company if different from CLS*

Index Sheet:	
Context:	
Keywords:	[Mots clés]
Hyperlink:	

Distribution:		
Company	Means of distribution	Names
CLS	Notification	

List of tables and figures

List of tables:

Aucune entrée de table d'illustration n'a été trouvée.

List of figures:

Figure 1: The mode mask, uploaded to CryoSat-2 in July 2012 (left panel) and January 2013 (right panel) (from *http://cryosat.mssl.ucl.ac.uk/qa/mode.php*) with the selected box areas. 2

Figure 2: Mean misfit curve for CPP (plotted in red) and ESRIN solution (plotted in yellow) as function of SWH in July 2012 over the Pacific SAR-mode area. 6

Figure 3: Mean misfit curve for CPP (plotted in red) and ESRIN solution (plotted in yellow) as function of SWH in July 2012 (left panel) and January 2013 (right panel) over the Pacific + NE Atlantic SAR-mode areas. 6

Figure 4: Mean of waveforms residuals (plotted in blue) with respect to SAR models from the CPP retracking algorithm for various SWH ranges [SWH-0.1m;SWH+0.1m]. The Y axis is the ratio (in percentage) of the residuals compared to the maximum of the mean waveform. The number of averaged waveforms is indicated for each subplot. 7

Figure 5: Mean SLA spectrum for CPP (plotted in blue) and ESRIN solution (plotted in red) in January 2013 over the entire SAR-mode area. The abscissa represents the wavelengths (on the top of the plot) or equivalently the wavenumbers (1/km)..... 8

Figure 6: ESRIN SAR solution (in red) and CPP (in blue) SLA profiles in July 2012 over Pacific..... 9

Figure 7: Histogram of 20-Hz SLA for the ESRIN SAR solution (in red) and CPP (in blue) in January 2013 (ascending passes)..... 9

Figure 8: Dependencies of 20-Hz range residual with filtered SWH, in July 2012 (ascending passes). Density of points in right panel. 10

Figure 9: Dependencies of 20-Hz range residual range with filtered SWH, in July 2012 (descending passes). Density of points in right panel.....10

Figure 10: Dependencies of 20-Hz range residual with filtered SWH, in January 2013 (ascending passes). Density of points in right panel. 10

Figure 11: Dependencies of 20-Hz range residual with filtered SWH, in January 2013 (descending passes). Density of points in right panel.....11

Figure 12: Dependencies of 20-Hz range residual with filtered SWH and radial velocity in July 2012 (left panel) and January 2013 (right panel). 11

Figure 13: Dependencies of 20-Hz range residual with across-track mispointing angle and filtered SWH in July 2012 (left panel) and January 2013 (right panel).....12

Figure 14: Dependencies of 20-Hz range residual with along-track mispointing angle and filtered SWH in July 2012 (left panel) and January 2013 (right panel). 12

Figure 15: SSH C2/C2 crossover residual using the ESRIN SAR solution retracker (top panel) and the CPP SAR retracker (bottom panel), averaged at crossovers averaged in (4degx4deg) geographical bins in July 2012 and January 2013 over the Pacific SAR-mode area. 13

Figure 16: Number of C2/C2 crossovers in July 2012 and January 2013 over the Pacific SAR-mode area. 13

Figure 17: Gain in variance of SSH C2/J2 crossover residual in July 2012 and January 2013 over the Pacific SAR-mode area. 14

Figure 18: Difference of range from ESRIN SAR solution and CPP retrackers (top panel) and map of SWH in July 2012 (bottom panel) for descending passes. 15

Figure 19: Difference of range from ESRIN SAR solution and CPP retrackers (top panel) and map of SWH in January 2013 (bottom panel) for descending passes. 16

Figure 20: ESRIN SAR solution (in red) and CPP (in blue) SLA profiles in July 2012 over the North East Atlantic area. Shaded region corresponds to land. 17

Figure 21: SLA statistics (mean, number of points, standard deviation) as function of the distance to the coast by using the ESRIN SAR solution (in red) and CPP (in blue) retrackers in ascending (left panel) and descending (right panel) passes. 17

Figure 22: Mean SWH spectrum for CPP (plotted in blue) and ESRIN solution (plotted in red) in January 2013 over the entire SAR-mode area. The abscissa represents the wavelengths (on the top of the plot) or equivalently the wavenumbers (1/km)..... 18

Figure 23: Histogram of 20-Hz SWH from ESRIN SAR solution (in blue), CPP (in red) and Jason-2 LRM MLE4 (in green) in July 2012. 19

Figure 24: SWH from CPP product (left panel) and Jason-2 (right panel) in July 2012 (unit in meter). 19

Figure 25: Dependencies of 20-Hz SWH residual with filtered SWH, in July 2012 and January 2013. Density of points in right panel. 20

Figure 26: Dependencies of 1-Hz SWH residual with filtered SWH (left panel), and bias between 1-Hz SWH estimates (right panel) in July 2012 and January 2013..... 20

Figure 27: Precision of 20-Hz SWH as function of SWH. 21

Figure 28: Dependencies of 20-Hz SWH residual with filtered SWH and radial velocity in January 2013 for ascending (left panel) and descending (right panel) passes. 21

Figure 29: Dependencies of 20-Hz SWH residual with across-track (left panel) and along-track (right panel) mispointing angle and filtered SWH in January 2013 for ascending passes. 22

Figure 30: Difference of SWH from ESRIN SAR solution and CPP retrackers (top panel) and map of SWH in July 2012 (bottom panel) for descending passes. 23

Figure 31: Difference of SWH from ESRIN SAR solution and CPP retrackers (top panel) and map of SWH in January 2013 (bottom panel) for ascending passes. 24

Figure 32: Mean sigma0 spectrum for CPP (plotted in blue) and ESRIN solution (plotted in red) in January 2013 over the entire SAR-mode area. The abscissa represents the wavelengths (on the top of the plot) or equivalently the wavenumbers (1/km). 25

Figure 33: Histogram of 20-Hz Sigma0 from ESRIN SAR solution (in green and blue) and CPP (in red) in January 2013 for ascending (left panel) and descending (right panel) passes. 25

Figure 34: Dependencies of 20-Hz sigma0 residual with filtered SWH, in July 2012 and January 2013. Density of points in right panel. 26

Figure 35: Dependencies of 20-Hz SIG0 residual (in dB unit) with filtered SWH and radial velocity in January 2013 for ascending (left panel) and descending (right panel) passes. 27

Figure 36: Dependencies of 20-Hz sigma0 residual (in dB unit) with across-track (left panel) and along-track (right panel) mispointing angles and filtered SWH in January 2013 for descending passes. 27

Figure 37: Difference of sigma0 from ESRIN SAR solution and CPP retrackers (top panel), and maps of different parameters in the following order: SWH, across-track mispointing angle and radial velocity, in January 2013 for descending passes. 29

Figure 38: Along-track sigma0 (top panel) and smoothed SAR-mode sigma0 (bottom panel) as function as latitude. Sigma0 from CPP SAR retracker is in blue, sigma0 from ESRIN SAR solution retracker in green and RDSAR-mode sigma0 in red. 30

Figure 39: Along-track sigma0 difference as function of latitude. Residual between smoothed CPP SAR-mode sigma0 and RDSAR-mode sigma0 is in blue, and residual between smoothed ESRIN SAR-mode sigma0 and RDSAR-mode sigma0 in green. 31

Figure 40: Difference between smoothed SAR-mode sigma0 and RDSAR-mode sigma0 as function of SWH, in July 2012 and January 2013. The red curve represents the mean of this difference. 31

Applicable documents

Reference documents

RD 1 Manuel du processus Documentation
CLS-DOC

Acronyms List

CLS	Collecte Localisation Satellite
CPP	Cryosat Processing Protoype
ESA	European Space Agency
ESRIN	European Space Research Institute
LRM	Low Resolution Mode
NA	Not Applicable
MQE	Mean Quadratic Error
PTR	Point Target Response
RD	Reference Document
RDSAR	Reduced Synthetic Aperture radar
SAMOSA	SAR Altimetry MOde Studies and Applications
SAR	Synthetic Aperture radar
SIRAL	Synthetic Aperture Interferometric Radar Altimeter
SLA	Sea level Anomalies
SSH	Sea Surface Haight
SWH	Significant Wave Height

List of Contents

1. Introduction 1
1.1. Purpose and scope 1
1.2. Document structure 1
2. Data and method overview 2
2.1. Data coverage and period 2
2.2. Method description 3
2.2.1. SAMOSA SAR solution (ESRIN) 3
2.2.2. CPP SAR numerical retracker 3
2.2.3. Edited data 4
3. Validation results and overall assessment 4
3.1. Performances of the waveform fitting 5
3.1.1. Misfit analysis 5
3.1.2. Waveform residuals 6
3.2. Comparison of range estimates 8
3.2.1. Spectral analysis of the SLA 8
3.2.2. SLA Histogram 9
3.2.3. Dependencies between parameters 9
3.2.4. Gain of variance of SSH 12
3.2.5. SLA cartography 14
3.2.6. SLA analysis in coastal ocean 16
3.3. Comparison of significant waveheight estimates 18
3.3.1. Spectral analysis of the SWH 18
3.3.2. SWH Histogram 18
3.3.3. Dependencies between parameters 19
3.3.4. Gain of variance of SSH 22
3.3.5. SWH cartography 22
3.4. Comparison of backscatter coefficient estimates 24
3.4.1. Spectral analysis of sigma0 24
3.4.2. Sigma0 Histogram 25
3.4.3. Dependencies between parameters 26
3.4.4. Sigma0 cartography 27
3.4.5. Comparison with RDSAR Sigma0 30
4. Conclusion 32
5. References 32

1. Introduction

1.1. Purpose and scope

This document aims at analysing the SAMOSA re-tracker solution from ESRIN for the CryoSat-2 mission, in comparison with the one implemented within the CPP chain that was statistically validated on real data. A set of dedicated diagnoses has been used to evaluate the quality of this retracking algorithm, and see if biases and noise performance computed for different estimated parameters are found to be consistent with those obtained from CPP or even better.

The description and the analysis of all the differences that are reported herein were discussed in a strong scientific collaboration with the algorithm expert/responsible who provides a very useful support to assess the performances of their algorithm, help to identify any unexpected behaviours and finally validate the content of this report.

1.2. Document structure

This document is structured into an introductory chapter followed by three chapters describing:

- the data used and coverage, and a short description of the two retracking algorithm to be compared (section 2),
- the analysis of the SAR L2 products through different diagnoses that are used to establish their performance (quantifying their skills and drawbacks) and their difference (section 3), and
- a discussion about these results (section 4).

2. Data and method overview

2.1. Data coverage and period

The ESRIN SAR solution was cross-compared with the validated CryoSat Processing Protoype (CPP) SAR L2 products over large areas operated in SAR mode: the equatorial Pacific and North East Atlantic oceans, for the following two periods: July 2012 and January 2013, as shown in Figure 1.

The equatorial Pacific area was selected by ESA among those proposed by an expert validation group, considering that the zone met the following criteria required:

1. low ocean variability (so easing the inter-mission calibration with conventional altimetry satellites like Jason 2),
2. few occurrences of rain and sigma-0 blooms events (which could have different impacts on SAR and RDSAR),
3. mean SWH around 2 meters and mean wind around 7 ms^{-1} (so the sea state is close to the mean conditions).

This site has been used for successfully validating the CPP SAR data, in comparison with the reduced SAR (RDSAR) data that provide a LRM reference over identical sea state [Moreau, 2013], [Labroue, 2014].

The North East Atlantic area is an additional pool of useful data with varying sea state conditions (very low wave heights in July and very high wave-heights in January), providing a much wider range of ocean wave heights for undertaking this study.

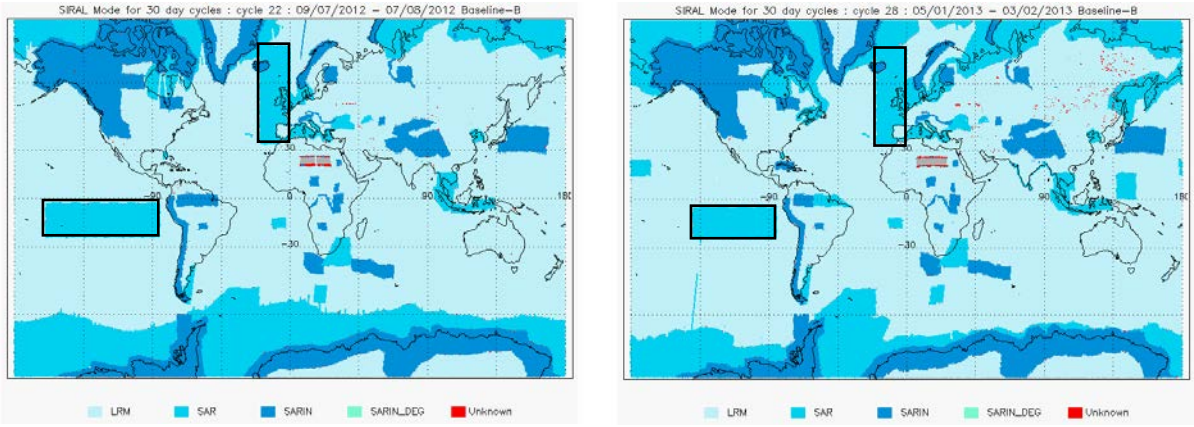

Figure 1: The mode mask, uploaded to CryoSat-2 in July 2012 (left panel) and January 2013 (right panel) (from http://cryosat.mssl.ucl.ac.uk/qa/mode.php) with the selected box areas.

The 20-Hz geophysical parameters (range, significant wave height, and sigma-0) retracked by the ESRIN SAR solution are obtained from the CPP multilooked echo power. These estimated parameters are thus generated at the same time and along-track location as the ones processed by the SAR CPP numerical retracker,

allowing both retrievals to be directly subtracted without the need to apply any geophysical model (e.g., wet and dry troposphere correction, ionosphere correction, tidal correction, dynamic atmospheric correction) or orbit elements (like the orbital ephemerides to derive a precise altitude) that may contribute to differences and lead to unclear conclusions regarding the comparison between the different processing approaches. This is especially true for the sea level anomaly (SLA) and other altimeter derived products like the wind measurements that account for corrections and/or models.

2.2. Method description

2.2.1. SAMOSA SAR solution (ESRIN)

The ESRIN SAR retracker solution is based on the use of the SAMOSA2 (SAR Altimetry MOde Studies and Applications) analytical model [Cotton and Martin-Puig, 2012] that is configured with the following parameters [Dinardo and Lucas, 2014]:

- Model antenna pattern is a 2-D Gaussian with teta3b_X=1.095°, teta3db_Y=1.22°
- Thermal Noise is computed from the first samples of the echo
- Along/cross off-nadir angles provided in the CPP products, are used as input parameters of the retracking scheme
- 212 Doppler looks accumulated for the multi-looking
- Scattering amplitude decay rate (nu) set to zero
- Slope effect and skewness effect set to zero
- a best-fitting algorithm based on the bounded Levenberg–Marquardt least square estimator

Adaptations were also needed to make the SAMOSA SAR model consistent with the real CryoSat-2 SAR echoes from CPP:

- Truncating the Doppler beams with zero (beyond the radar receiving window) before the range alignment operation
- Applying Look-up table under iteration to correct the approximations for the point target response (PTR)

2.2.2. CPP SAR numerical retracker

The CPP SAR numerical retracker [Boy and Moreau, 2013] is a standard least squares estimator (LSE) consisting in fitting a multi-looked SAR waveform with a 3-parameters echo model (range, significant wave height, amplitude), that is pre-computed off-line by an amplitude numerical simulator [Desjonquères et al., 2012].

The amplitude simulator model mimics the Cryosat-2 altimeter response in SAR-mode (taking into account the real elliptical antenna pattern and a real point target response). It is based on a point-by-point radar response simulation on a gridded surface without limitation of resolution (fully adaptive), accounting for the satellite altitude and the altimeter characteristics of the mission. This approach

may be considered to be more robust than analytical ones, particularly when faced with atypical observations (e.g., elliptical antenna pattern, off-nadir mispointing angles, point target response) that are difficult to put into equations.

The CPP SAR numerical retracker accounts for varying off-nadir mispointing angles in both axes (along-track and cross-track directions) as input parameters. Those angles are obtained from the star tracker information, roll and pitch angles, and compensated by pre-computed angular biases corresponding to the angular alignment between the star tracker boresight and the altimeter electromagnetic axis.

This solution is currently implemented in the CPP chain.

2.2.3. **Edited data**

Data editing is necessary to remove altimeter measurements having lower accuracy. To analyze the consistency between both retracker solutions in open ocean, only valid ocean data are selected (removing data corrupted by sea ice and rain). The following editing criteria are applied:

- a valid flag is used, based on the validation task of CryoSat-2 performed by the CLS Space Oceanography Division, ensuring to eliminate all outliers (that may be related to some spurious observations caused by rain, blooms, or to some specifics events that can occur for instance after an orbit maneuver, or when an anomaly on an instrument impacts the quality of the measurement)
- data points close to the shoreline are edited (distance to coast <10km)
- more specific editing criteria, based on thresholds on different parameters are applied to filter out data points:
    - 0.1m<SWH and SWH>10m are removed,
    - Only corrected SLA between -2m and +2m are considered

3. **Validation results and overall assessment**

The overall objective of this validation exercise is to assess the performances of the innovative ESRIN SAR retracker solution, highlighting the main features, discrepancies, advantages and drawbacks of this method while comparing to the CPP SAR products.

The assessment task is conducted with robust and standard methods that are classically used in current Cal/Val analyses, to precisely validate and cross-calibrate different algorithms on the same measurement data set (same altimeter mission, same selected areas and time frames).

For this purpose, the validation of the ESRIN SAR solution is performed through the following set of diagnoses:

- Estimated parameters cartography to visualize their geographic locations and identify their dependencies on geophysical signals (SWH, calms or

sigma-0 blooms or rain areas, but also mispointing angles and vertical velocity);

- Map of reduction of sea surface height (SSH) variance at crossovers (C2/C2 and C2/J2) to determine which algorithm shows the best performances;

- Diagnoses on the performances of the waveform fitting (plot of the misfit and plots of the residuals between the measured waveforms and the fitted model as a function of SWH);

- Plots of the parameters themselves (parameter profiles as a function of time, histograms, dispersions or scatter-plots);

- Spectral analysis of parameters (sea level anomalies, SWH or sigma-0);

- Analysis of the retracking algorithms in the coastal domain.

These diagnoses are performed at higher data set rhythm, 20-Hz.

3.1. Performances of the waveform fitting

3.1.1. **Misfit analysis**

A first interesting diagnostic for this comparison consists in evaluating the mean quadratic error (MQE), which measures the misfit of the SAR models to the echo waveforms. This indicator allows to evaluate the accuracy of the retracking algorithm to model real echoes, that can impact the quality of the estimates.

Figure 2 represents the mean MQE (i.e. misfit averaged on an SWH interval) of the ESRIN SAR solution and CPP retrackers at 20-Hz, over the Pacific SAR box in July 2012. Figure 3 plot the mean MQE over the entire selected area in July 2012 (right panel) and January 2013 (right panel). These plots show a good agreement between both solutions, but with a noticeable lower mean misfit of the CPP than the SAMOSA ESRIN solution one. They tend to be coincident for high SWH as expected (where the effect of the Gaussian approximation of the PTR becomes negligible).

Otherwise the misfit cloud for CPP and SAMOSA ESRIN solution covers each other totally, exhibiting a very similar behaviour.

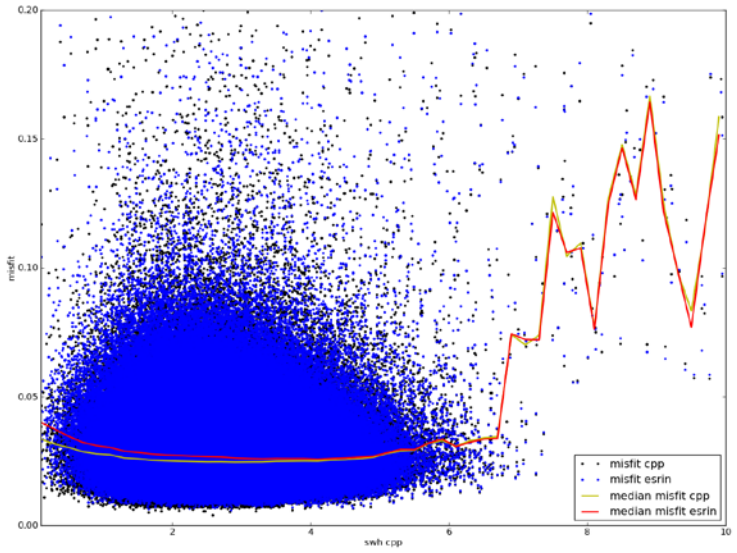

Figure 2: Mean misfit curve for CPP (plotted in red) and ESRIN solution (plotted in yellow) as function of SWH in July 2012 over the Pacific SAR-mode area.

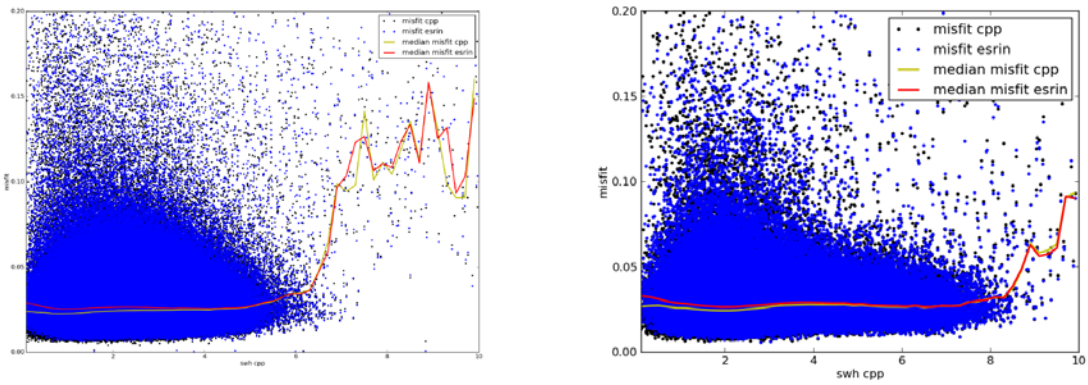

Figure 3: Mean misfit curve for CPP (plotted in red) and ESRIN solution (plotted in yellow) as function of SWH in July 2012 (left panel) and January 2013 (right panel) over the Pacific + NE Atlantic SAR-mode areas.

3.1.2. Waveform residuals

We computed the mean CPP waveforms residuals on hundreds of measurements in July 2012 over the Pacific SAR-mode area, in order to better characterize the location of the main discrepancies in the waveform between the SAR-mode echo waveforms and the waveform models, for different classes of SWH. On Figure 4, it can be observed that greatest errors are obtained at the toe and in the leading edge of the waveform, where the amplitude of the signal is high. Also, one can see that residuals in percentage are noticeable in the trailing edge, but with normally

lower impact in the fitting scheme, since the amplitude of the waveform in this part is not significant.

In addition, the residuals seem to be most important at very low (1m) and particularly very high wave heights as expected.

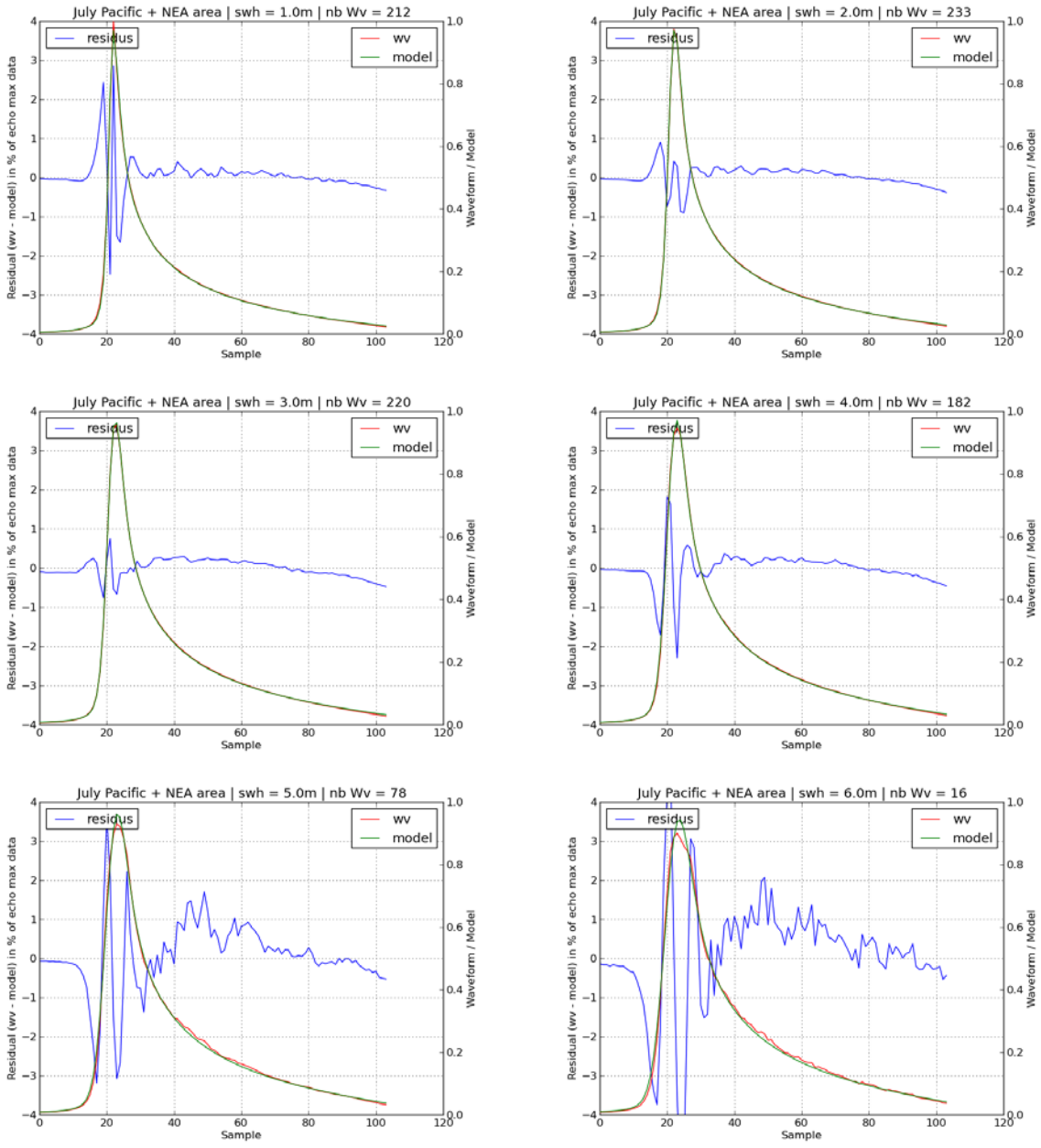

Figure 4: Mean of waveforms residuals (plotted in blue) with respect to SAR models from the CPP retracking algorithm for various SWH ranges [SWH-0.1m;SWH+0.1m]. The Y axis is the ratio (in percentage) of the residuals compared to the maximum of the mean waveform. The number of averaged waveforms is indicated for each subplot.

3.2. Comparison of range estimates

This section presents the results of the CLS analysis bench obtained with both algorithms (ESRIN SAR solution and CPP), to quantify the retracker performances. In the following subsection the range estimates have been compared through several metrics pointing out their similarities and discrepancies.

3.2.1. Spectral analysis of the SLA

On the SLA spectra (Figure 5), we can see that both retrackers measure exactly the same content of the oceanic signal from low to high wavelength. Also, one can notice that the SAR altimeter data is not affected by correlated errors that are seen on LRM-mode spectra (as a spectral hump). From this graph, it appears that the SAR SLA spectrum perfectly follows the slope of the oceanic signal up to 50 km, allowing 1-Hz product users to recover smaller wavelengths (10-80 km) of interest for oceanography, where conventional altimeter mode needs to use complex waveform processing, dedicated retrackers or post-processing (e.g. Singular Value Decomposition algorithm) to edit out spurious data from historical LRM datasets and reduce both the noise level and the spectral hump.

The two spectra are obtained by integration of many elementary spectra computed on continuous data segments, for which an averaged SWH of 2.5m is observed. The computed noise levels of the SLA from both solutions are around 5.5 cm at 20 Hz (the full altimetry resolution).

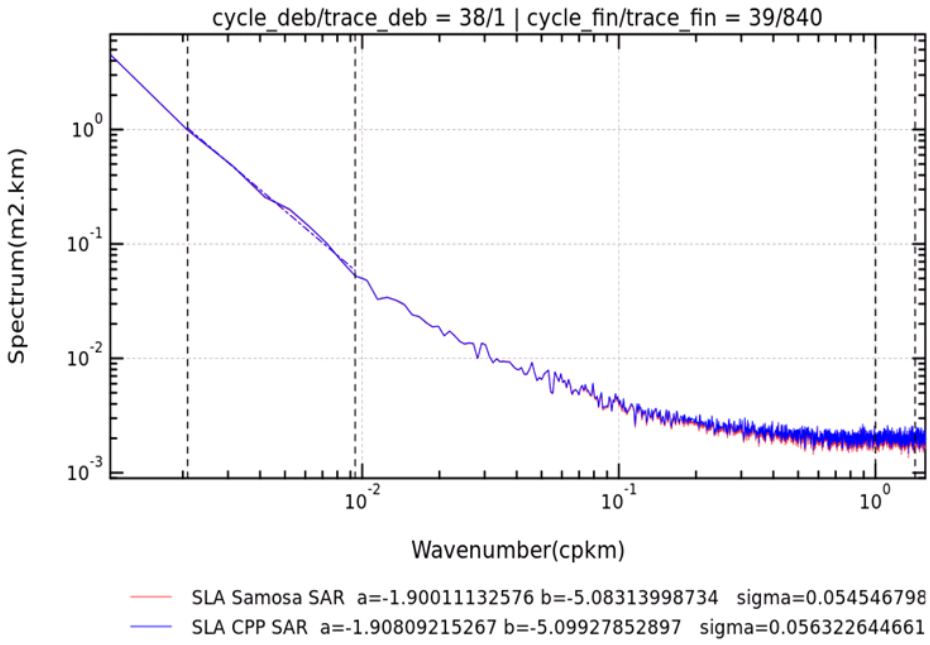

Figure 5: Mean SLA spectrum for CPP (plotted in blue) and ESRIN solution (plotted in red) in January 2013 over the entire SAR-mode area. The abscissa represents the wavelengths (on the top of the plot) or equivalently the wavenumbers (1/km).

We can see on Figure 6 that SLA signals from both retrackers are very consistent (two SLAs overlapped).

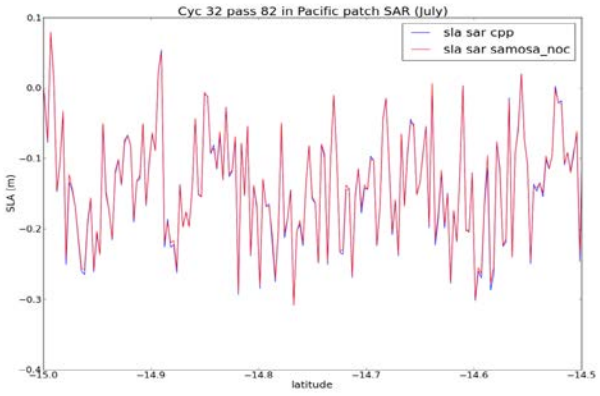

Figure 6: ESRIN SAR solution (in red) and CPP (in blue) SLA profiles in July 2012 over Pacific.

3.2.2. SLA Histogram

The comparison between the ESRIN SAR solution and CPP products underlines a very low global bias of near 3 mm in range.

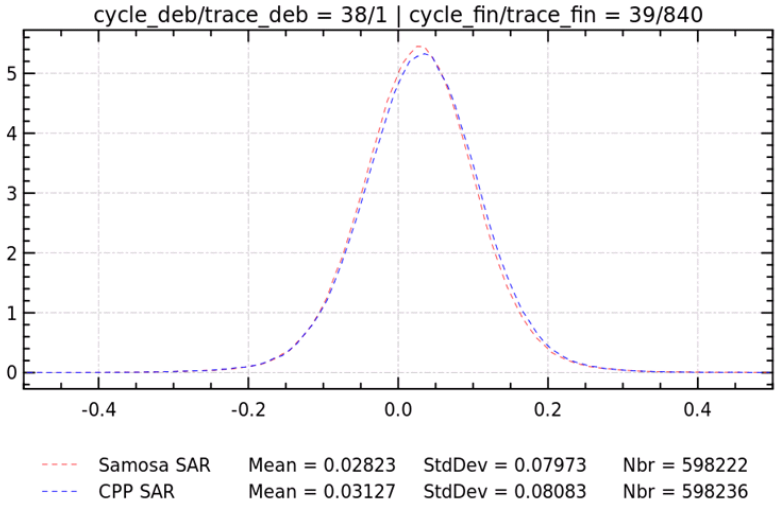

Figure 7: Histogram of 20-Hz SLA for the ESRIN SAR solution (in red) and CPP (in blue) in January 2013 (ascending passes).

3.2.3. Dependencies between parameters

The results are presented separating ascending and descending passes since the radial velocity and the mispointing angles come up with different values at the same location that may impact the estimates.

To assess the consistency between 20-Hz range calculated by the ESRIN SAR solution retracker and by CPP retracker, their difference (or residual) has been computed as function of the filtered SWH, for ascending and descending passes, in

July 2012 and January 2013. The following figures show that the residual is quite low between -5mm and +5mm for SWH up to 4m, in ascending and descending passes, and the two selected periods.

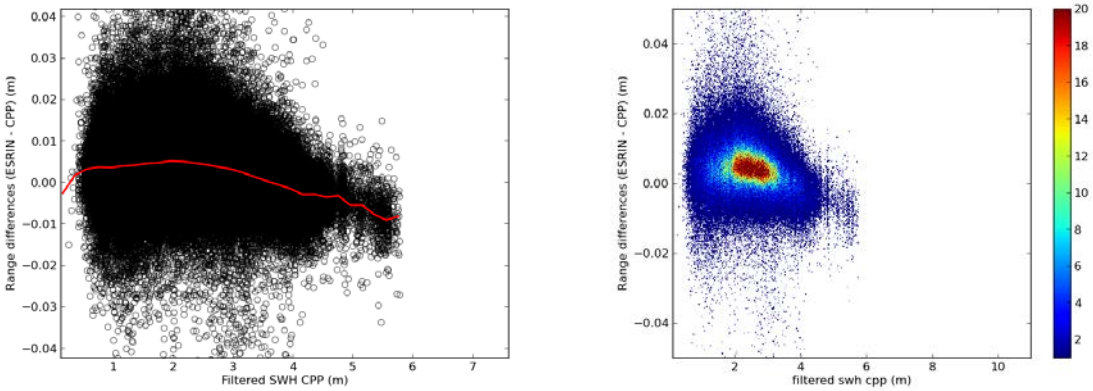

Figure 8: Dependencies of 20-Hz range residual with filtered SWH, in July 2012 (ascending passes). Density of points in right panel.

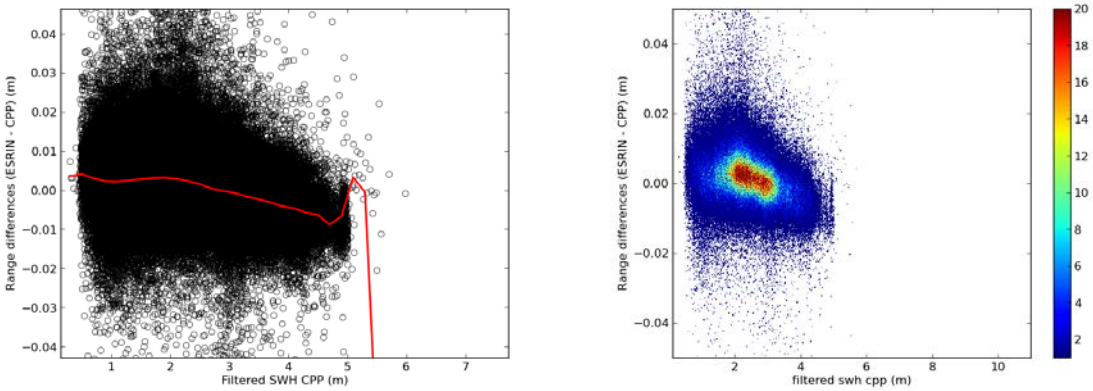

Figure 9: Dependencies of 20-Hz range residual range with filtered SWH, in July 2012 (descending passes). Density of points in right panel.

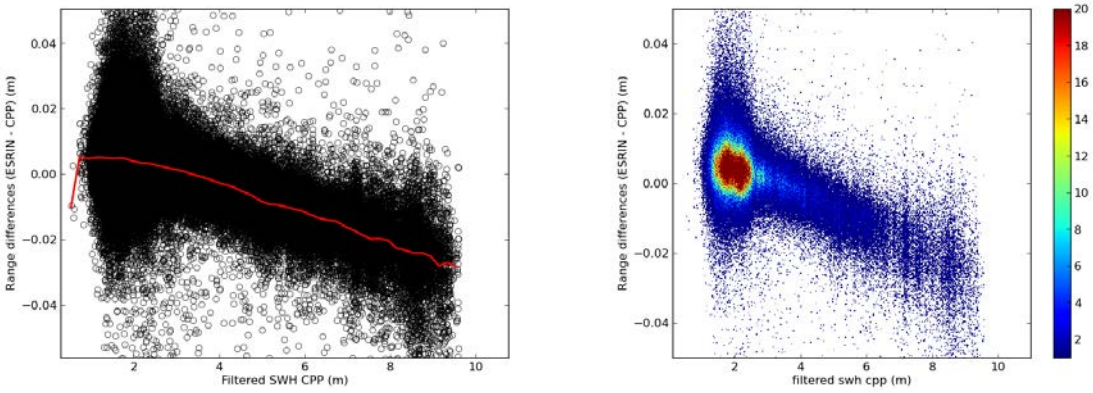

Figure 10: Dependencies of 20-Hz range residual with filtered SWH, in January 2013 (ascending passes). Density of points in right panel.

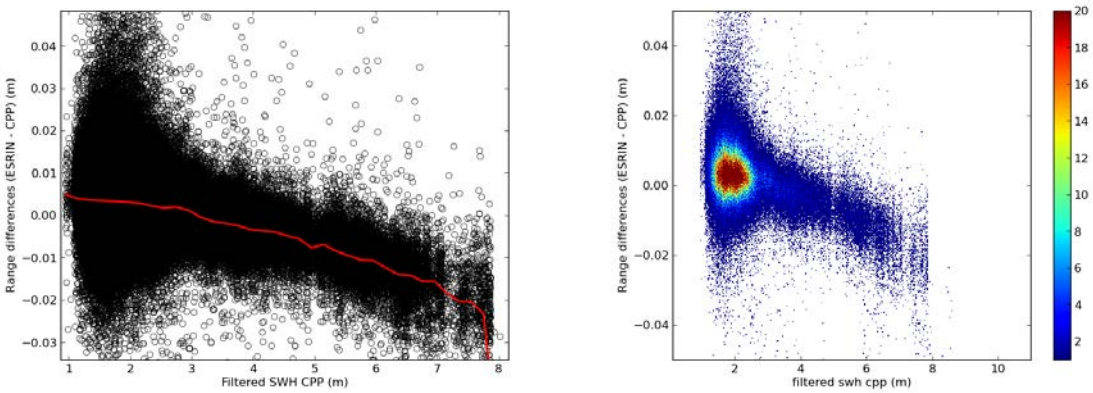

Figure 11: Dependencies of 20-Hz range residual with filtered SWH, in January 2013 (descending passes). Density of points in right panel.

The following diagnostics aim at identifying possible dependencies of the difference of 20-Hz ranges on the across-track mispointing angle, along-track mispointing angle or radial velocity.

In Figure 12, the residual is plotted versus SWH and the radial velocity. The Figure 13 and Figure 14 plot the same parameter as a function of the radial velocity and the across-track and along-track mispointing angles obtained from the star tracker information. Those results show that the ESRIN SAR solution retracker has no apparent impact on the dependencies of the residual measurements with respect to both mispointing angles and the radial velocity.

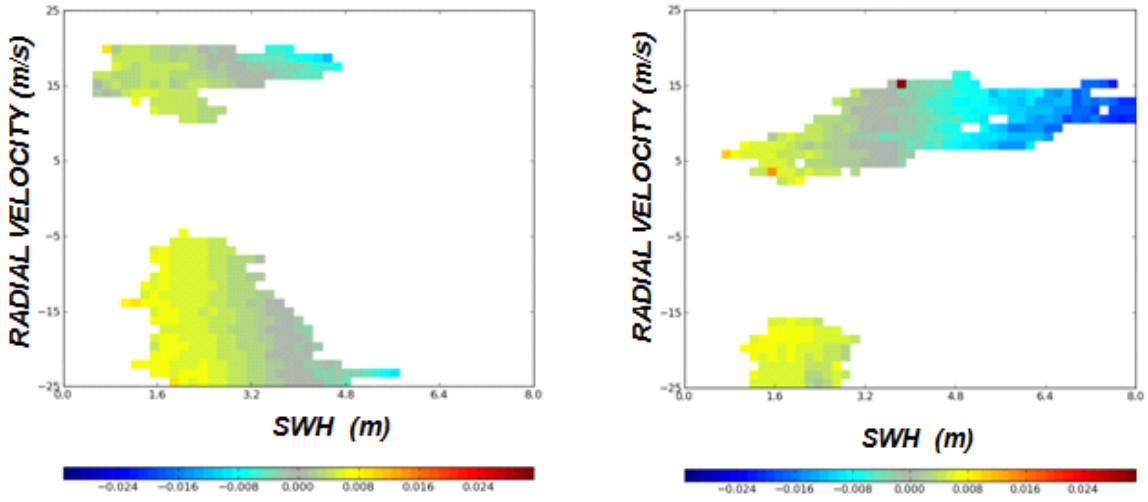

Figure 12: Dependencies of 20-Hz range residual with filtered SWH and radial velocity in July 2012 (left panel) and January 2013 (right panel).

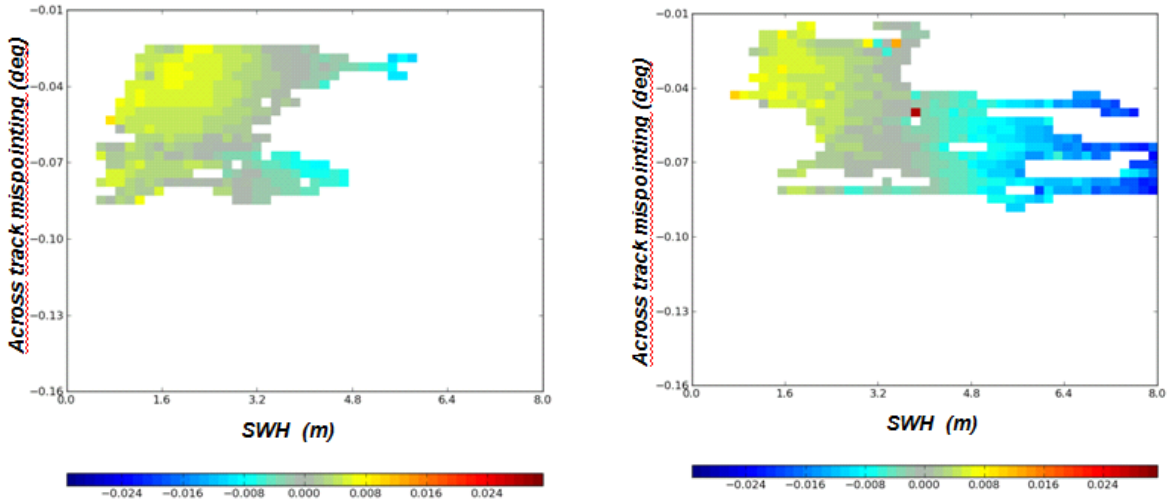

Figure 13: Dependencies of 20-Hz range residual with across-track mispointing angle and filtered SWH in July 2012 (left panel) and January 2013 (right panel).

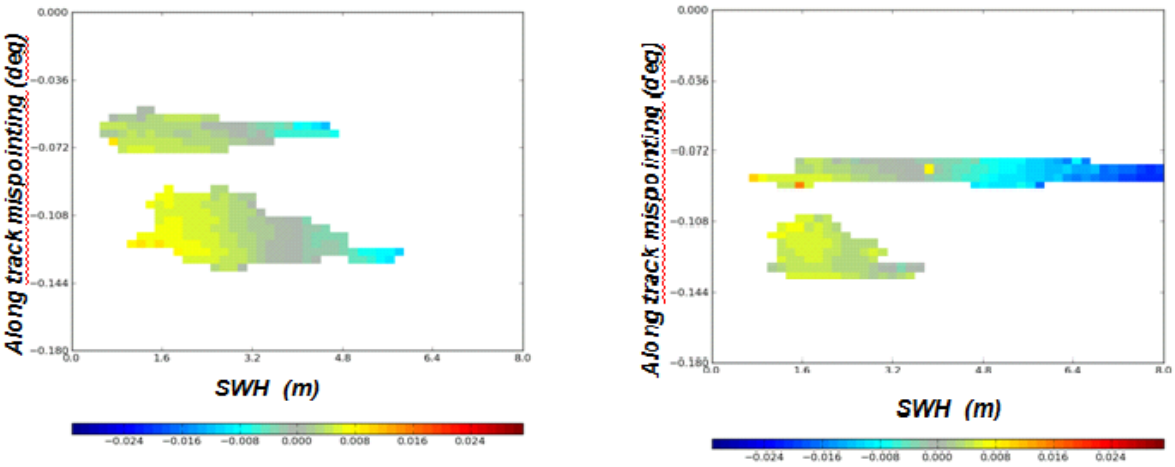

Figure 14: Dependencies of 20-Hz range residual with along-track mispointing angle and filtered SWH in July 2012 (left panel) and January 2013 (right panel).

3.2.4. Gain of variance of SSH

To quantify the system performances, we analyse the SSH variance reduction at C2/C2 crossovers between ascending and descending passes, that one can achieved with the ESRIN SAR solution retracker. This is performed by a direct analysis of the variance difference of the SSH between the two algorithm (ESRIN – CPP) solutions. A selection is done to only keep data with time tag differences lower than 10 days (between ascending and descending passes). This allows a minimization of the oceanic variability contribution.

Figure 15 shows the SSH residual at C2/C2 crossovers using the ESRIN SAR solution retracking (top panel) and the CPP retracking (bottom panel) output. No relevant analyses are to be expected from this figure since the number of C2/C2 crossovers is statistically very low (due to a very short selected period) as shown in Figure 16.

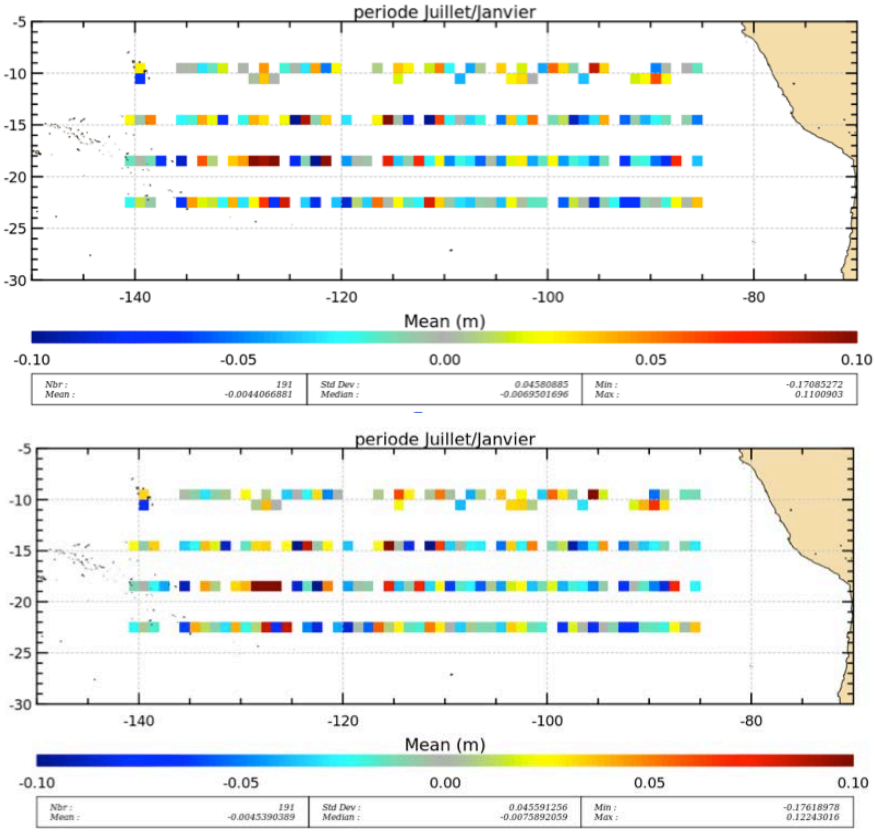

Figure 15: SSH C2/C2 crossover residual using the ESRIN SAR solution retracker (top panel) and the CPP SAR retracker (bottom panel), averaged at crossovers averaged in (4degx4deg) geographical bins in July 2012 and January 2013 over the Pacific SAR-mode area.

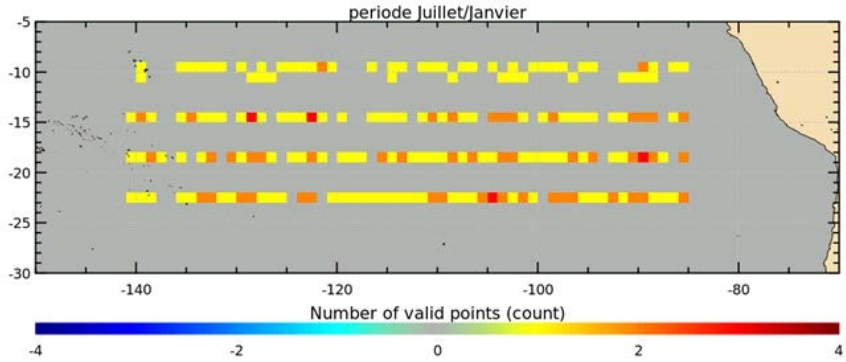

Figure 16: Number of C2/C2 crossovers in July 2012 and January 2013 over the Pacific SAR-mode area.

The computed global precision of the SSH C2/C2 crossover residual is equal to 5.2cm for both algorithms meaning that the variance of SSH ESRIN SAR solution and the variance of SSH CPP are similar and consequently that both algorithms have similar performances.

The same analysis has been done on C2/J2 crossovers. Figure 17 shows the corresponding gain in variance of SSH differences using the ESRIN SAR solution retracker and the CPP retracker output at crossover points with J2 LRM data selected on a sliding window of 10 days. The number of points is not statistically significant in 1°x1° geographical bins to reveal any apparent pattern and assess the SAR-mode retracking methods with crossover diagnostics. With the few data we do have, the variance difference of SSH computed from the global precision of the SSH C2/J2 crossover residual for both algorithms is negligible.

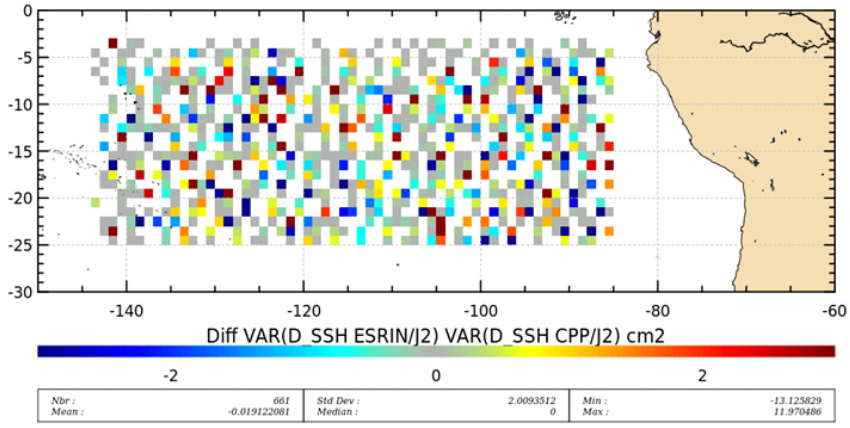

Figure 17: Gain in variance of SSH C2/J2 crossover residual in July 2012 and January 2013 over the Pacific SAR-mode area.

To conclude this part, no gain in SSH variance is observed which confirms that the two SAR-mode retracking algorithms are quite equivalent in open ocean as it is already highlighted. However an analysis of the reduction of the SSH crossover variance over a longer period and geographical area would permit to make this observation with confidence.

3.2.5. **SLA cartography**

The along track 20-Hz measurements are used to construct a mean map (averaged values in each 2°x2° grid bins) of the ESRIN SAR solution and CPP estimates, but also their differences and others parameters (in particular the radial velocity and the across-track and along-track mispointing angle that may impact the retrievals). In this way, we can easily observe the geographical distribution of those parameters and the mapping biases between retracking algorithms.

A global map of the range difference highlights this dependency (top panels of the Figure 18 and Figure 25) showing a clear correlation of the range difference with wave heights (Figure to be compared with bottom panels), though the range difference is low (up to ±5mm) for wave heights between 0 and 4m. Possible dependencies to others parameters are not seen.

Otherwise, it appears no evident dependence between the range difference and other parameters (such as the radial velocity and mispointing angles).

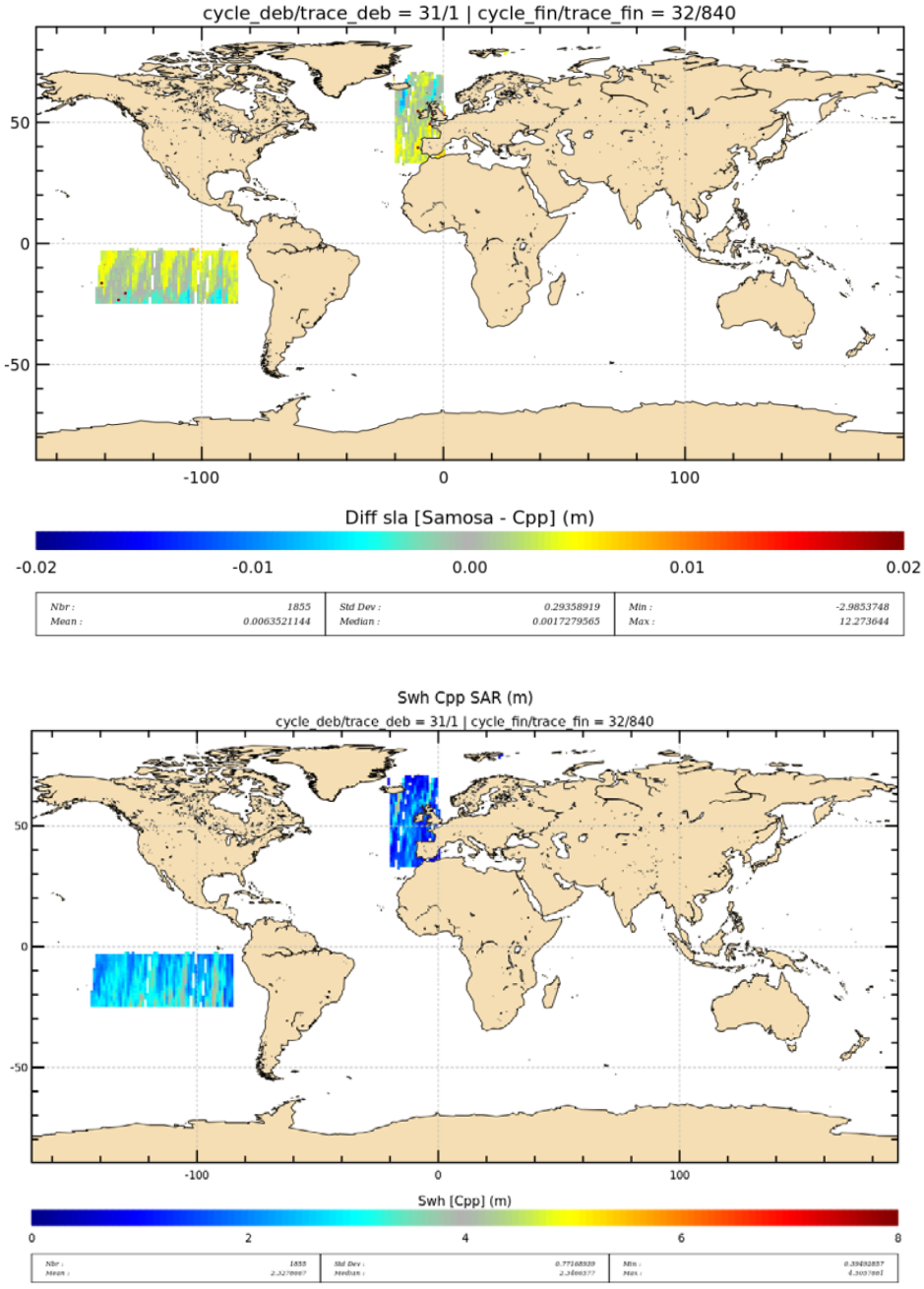

Figure 18: Difference of range from ESRIN SAR solution and CPP retrackers (top panel) and map of SWH in July 2012 (bottom panel) for descending passes.

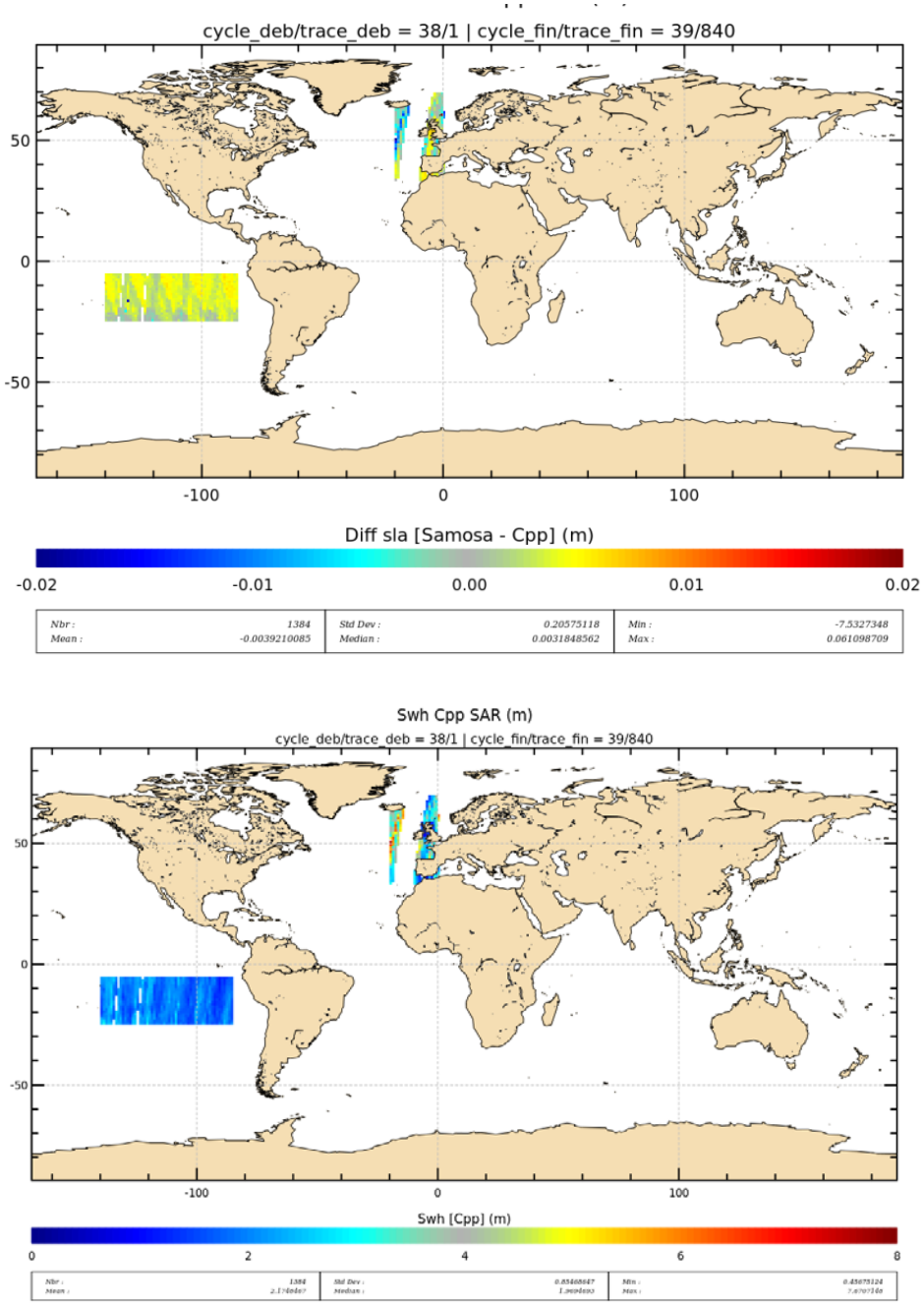

Figure 19: Difference of range from ESRIN SAR solution and CPP retrackers (top panel) and map of SWH in January 2013 (bottom panel) for descending passes.

3.2.6. SLA analysis in coastal ocean

It is also of importance to evaluate the ability of the retracking algorithms to run near the coasts. We can see on Figure 20 a quite similar behaviour with few non valid CPP estimates while approaching the coast.

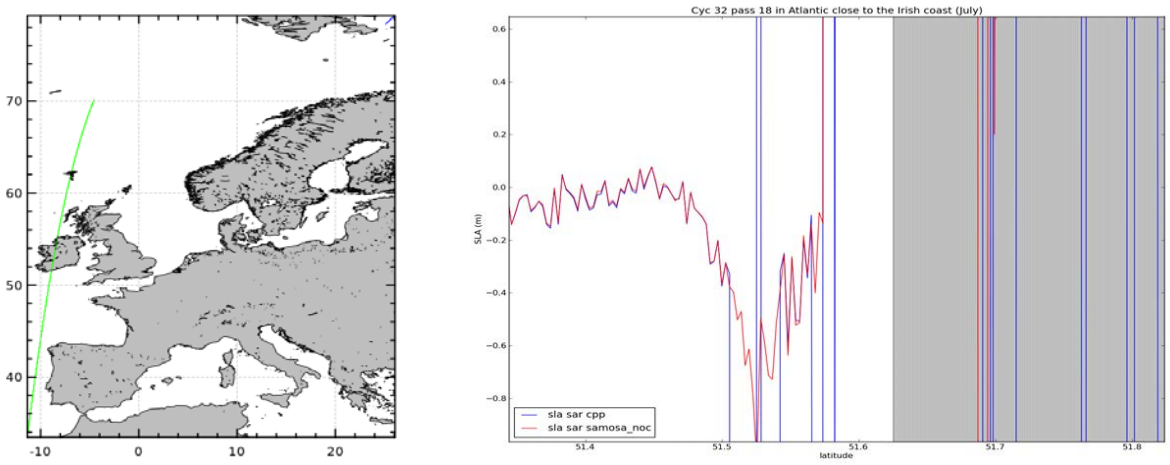

Figure 20: ESRIN SAR solution (in red) and CPP (in blue) SLA profiles in July 2012 over the North East Atlantic area. Shaded region corresponds to land.

This analyse is performed statistically over a large number of observations to assess the consistency of the two retracking algorithms in coastal region.

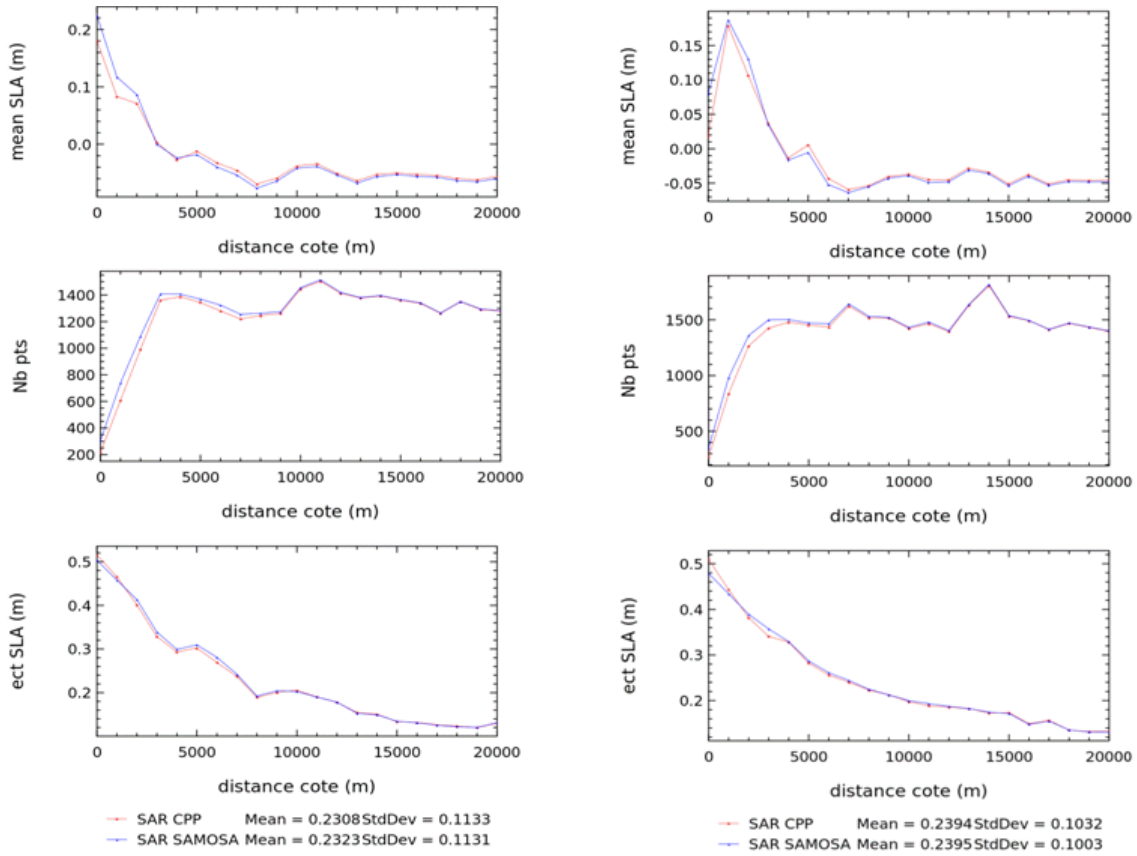

Figure 21: SLA statistics (mean, number of points, standard deviation) as function of the distance to the coast by using the ESRIN SAR solution (in red) and CPP (in blue) retrackers in ascending (left panel) and descending (right panel) passes.

Figure 25 shows the mean SLA between 0 and 20km from shoreline and the associated standard deviation. From this figure, it appears no clear differences between retracking estimates, only slight increase of the number of valid measurements near the coast with the ESRIN SAR solution retracker.

3.3. Comparison of significant waveheight estimates

The same analysis is done on significant wave height (SWH).

3.3.1. Spectral analysis of the SWH

On the Figure 22, one can see that the two spectra are well overlapped with each other. We also notice that the SWH noise level is around 42cm at 20 Hz for both retracking algorithms (1cm lower for the ESRIN solution).

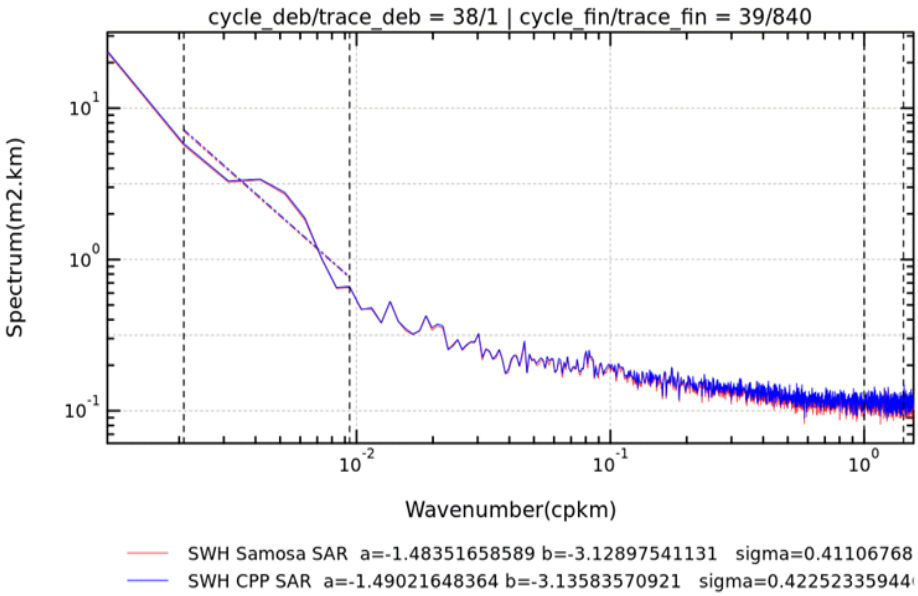

Figure 22: Mean SWH spectrum for CPP (plotted in blue) and ESRIN solution (plotted in red) in January 2013 over the entire SAR-mode area. The abscissa represents the wavelengths (on the top of the plot) or equivalently the wavenumbers (1/km).

3.3.2. SWH Histogram

Figure 23 shows the SWH histograms for the two SAR retracker solutions. One can observe very similar histograms and few cm (< 3cm) of difference with the Jason-2 SWH averaged in the same area and time period as shown in Figure 24. This result needs however to be precisely evaluated with larger amount of data.

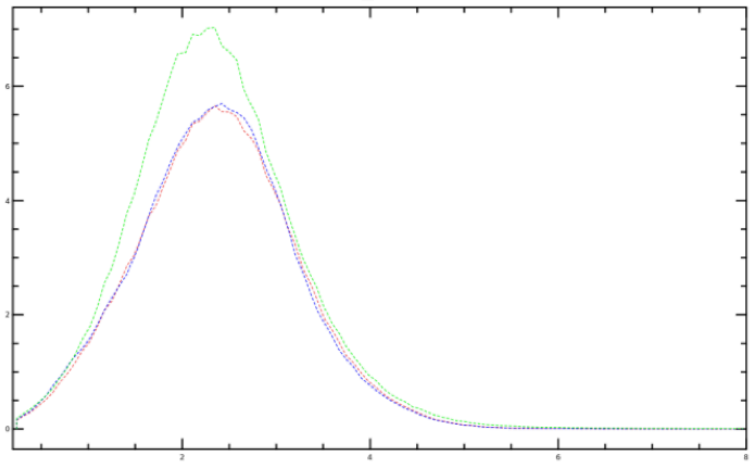

Figure 23: Histogram of 20-Hz SWH from ESRIN SAR solution (in blue), CPP (in red) and Jason-2 LRM MLE4 (in green) in July 2012.

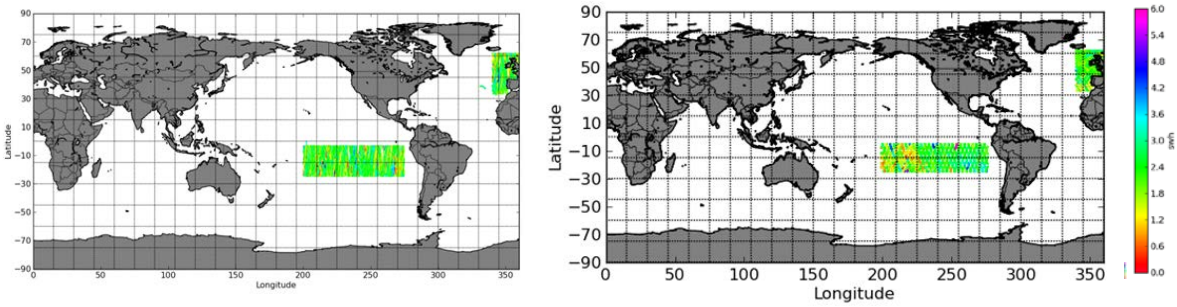

Figure 24: SWH from CPP product (left panel) and Jason-2 (right panel) in July 2012 (unit in meter).

3.3.3. **Dependencies between parameters**

Let's now analyse the sensitivity of the SWH residual to the across-track and along-track mispointing angles, the radial velocity and the wave height.

The Figure 25 shows that the mean 20-Hz SWH residual is non-significant over the entire wave height range (from low to high SWH) for the two selected periods. This is confirmed by the mean 1-Hz SWH residual plotted in Figure 26 (left panel). The linear regression from the SWH scatter-plot displayed in Figure 26 (right panel) also shows a very good agreement between the retracking SWH estimates with only 5cm at 4m SWH.

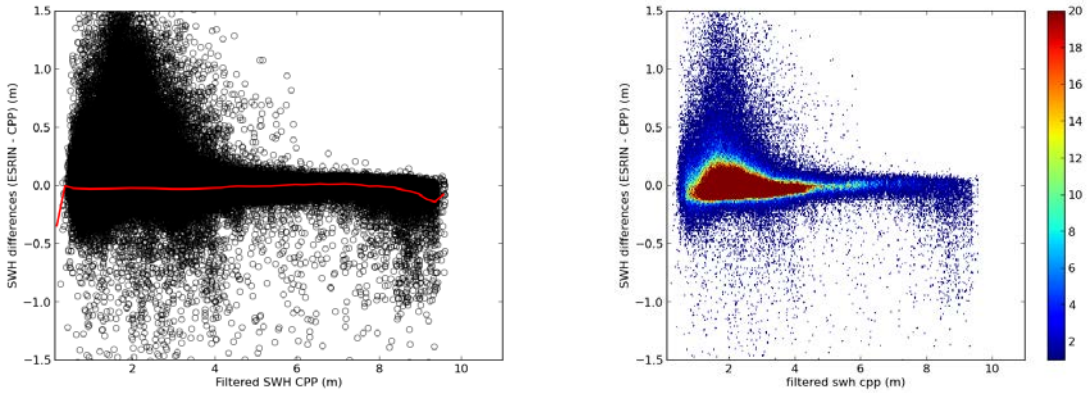

Figure 25: Dependencies of 20-Hz SWH residual with filtered SWH, in July 2012 and January 2013. Density of points in right panel.

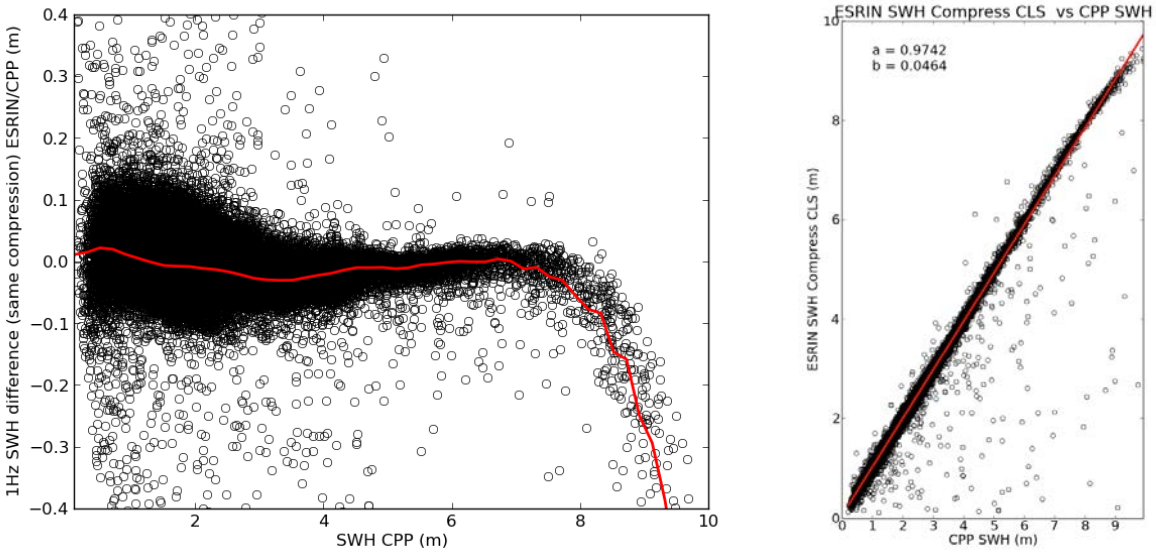

Figure 26: Dependencies of 1-Hz SWH residual with filtered SWH (left panel), and bias between 1-Hz SWH estimates (right panel) in July 2012 and January 2013.

Figure 27 exhibits the 20-Hz SWH noise as function of wave height for the two retracking algorithms. One can observe quite similar behaviour with around 40cm of SWH noises between 2-3m of wave height, as it was determined by the SWH spectral analysis. Discrepancies are only found at very low wave height (below 1m) where the CPP SWH noise drops quickly whereas the ESRIN solution retracker one remains almost unchanged (the first point is in error). For these particular waveforms, the CPP retracker may allow a noticeable better fit of the measurements, as it was already observed through misfit analysis.

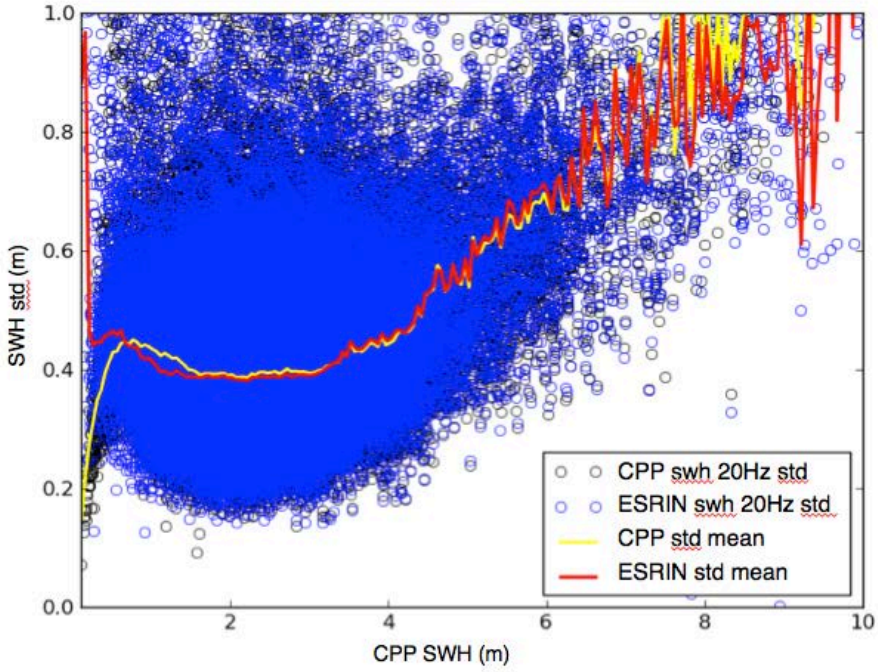

Figure 27: Precision of 20-Hz SWH as function of SWH.

In Figure 28 the 20-Hz SWH residual is plotted versus SWH and the radial velocity. Figure 29 plots the same parameter as a function of SWH and across-track mispointing angle and along-track mispointing angle. From these figures, one can observe that the ESRIN SAR solution retracker has no impact on the dependencies of the SWH residual measurements with respect to both mispointing angles and the radial velocity. However the SWH difference appears to be correlated to SWH. But considering the level of residuals that are observed, we may nearly neglect this small effect.

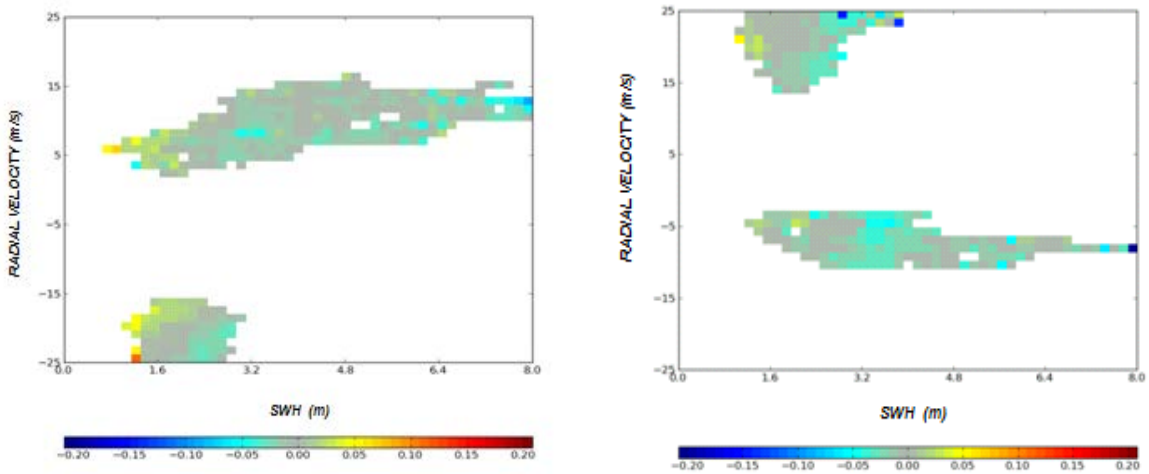

Figure 28: Dependencies of 20-Hz SWH residual with filtered SWH and radial velocity in January 2013 for ascending (left panel) and descending (right panel) passes.

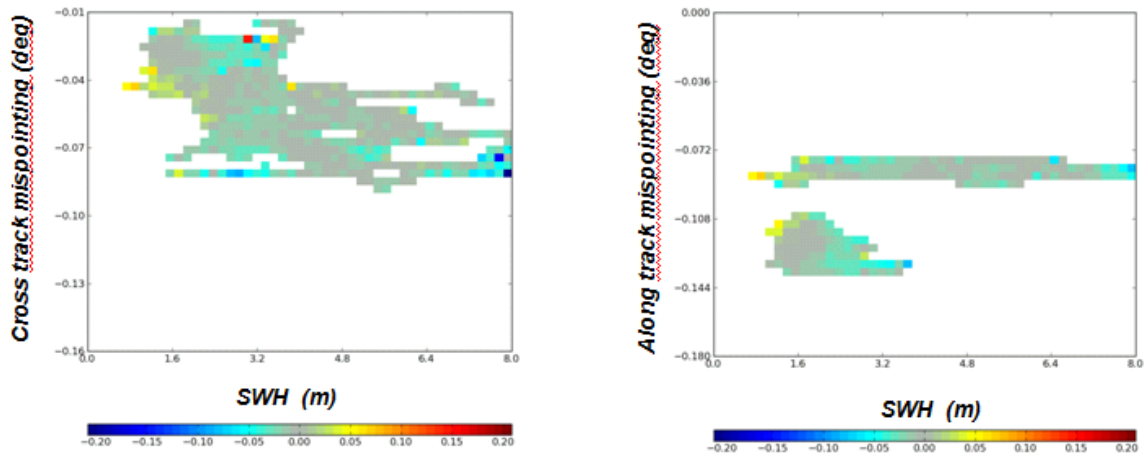

Figure 29: Dependencies of 20-Hz SWH residual with across-track (left panel) and along-track (right panel) mispointing angle and filtered SWH in January 2013 for ascending passes.

3.3.4. Gain of variance of SSH

The SWH analysis at crossovers is not relevant since the number of crossovers with a reduced time lag below 1-day (to insure similar sea state) is very limited (whereas a maximum of 10-days time lag is used for the SSH crossovers).

3.3.5. SWH cartography

A global map reveals (as for range differences) that the SWH residual is clearly correlated to the wave height (Figure 30 and Figure 31), though the SWH difference is low (as high as 5cm). Furthermore, no dependence between the SWH residual and other parameters (such as the radial velocity and mispointing angles) is reported.

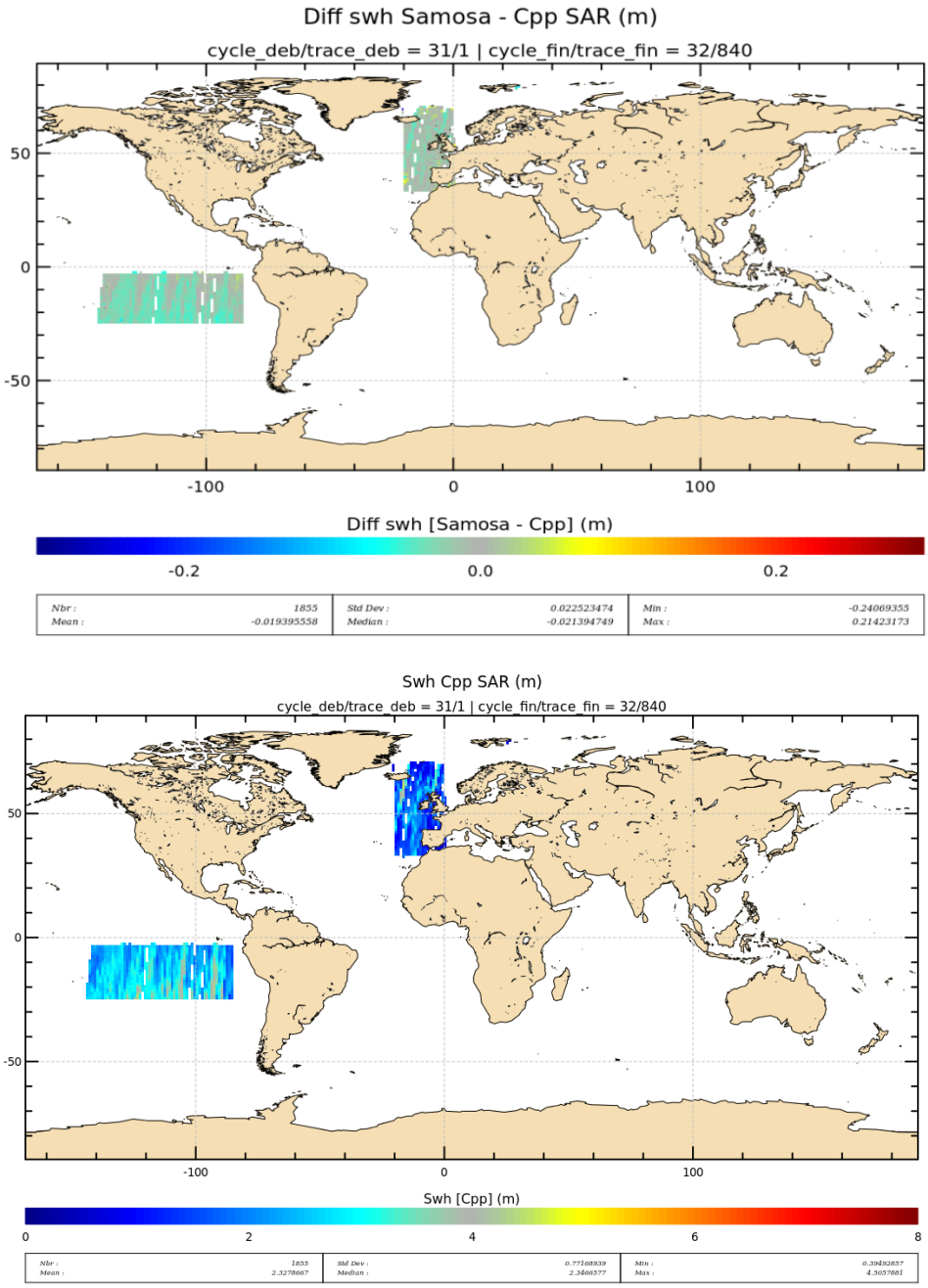

Figure 30: Difference of SWH from ESRIN SAR solution and CPP retrackers (top panel) and map of SWH in July 2012 (bottom panel) for descending passes.

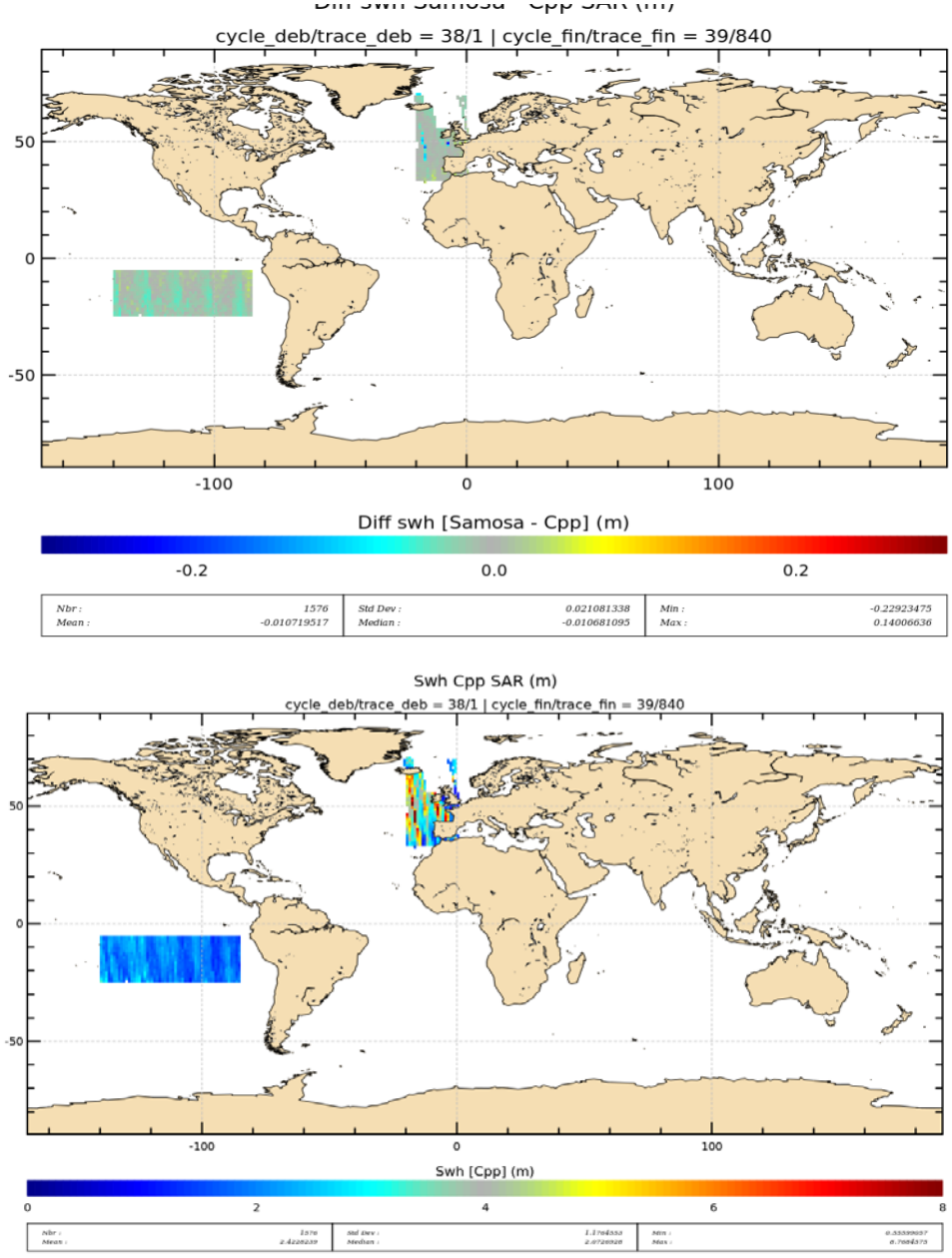

Figure 31: Difference of SWH from ESRIN SAR solution and CPP retrackers (top panel) and map of SWH in January 2013 (bottom panel) for ascending passes.

3.4. Comparison of backscatter coefficient estimates

The same analysis is done on backscatter coefficient (sigma0).

3.4.1. Spectral analysis of sigma0

As it was done for the other parameters, a spectrum analysis has been performed on sigma0 estimates from both retracking algorithms (Figure 32) showing two

spectra well overlapped with each other and no differences between sigma0 noise levels. This result indicates again similar behaviour of the retracking algorithms on geophysical signals from high to low wavelengths.

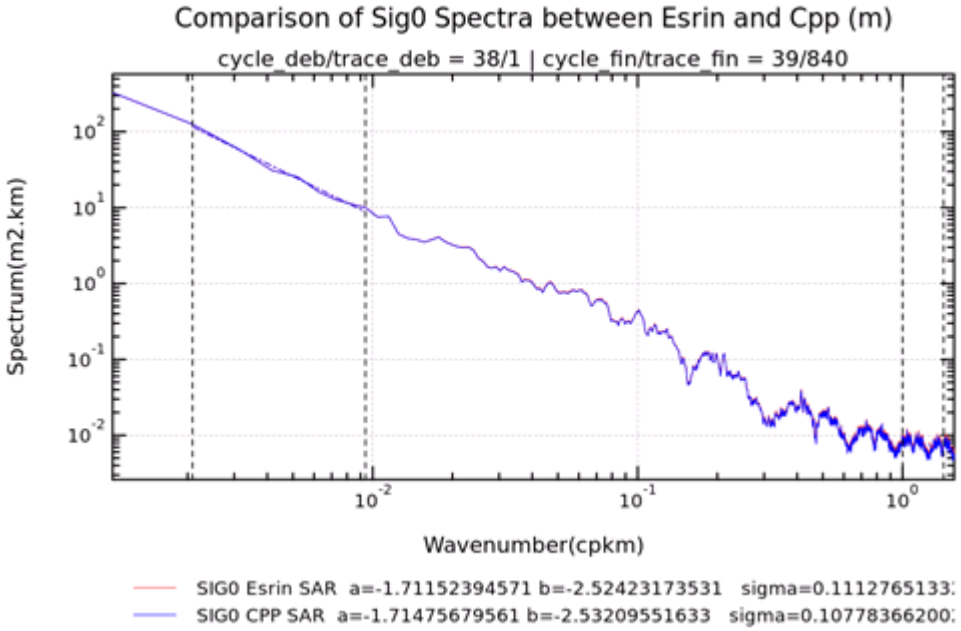

Figure 32: Mean sigma0 spectrum for CPP (plotted in blue) and ESRIN solution (plotted in red) in January 2013 over the entire SAR-mode area. The abscissa represents the wavelengths (on the top of the plot) or equivalently the wavenumbers (1/km).

3.4.2. Sigma0 Histogram

Figure 33 shows very similar sigma0 histograms. We also notice that the difference of sigma0 between ascending and descending passes is low, around 0.15dB and 0.1dB for the ESRIN solution retracker and the CPP SAR retracker respectively.

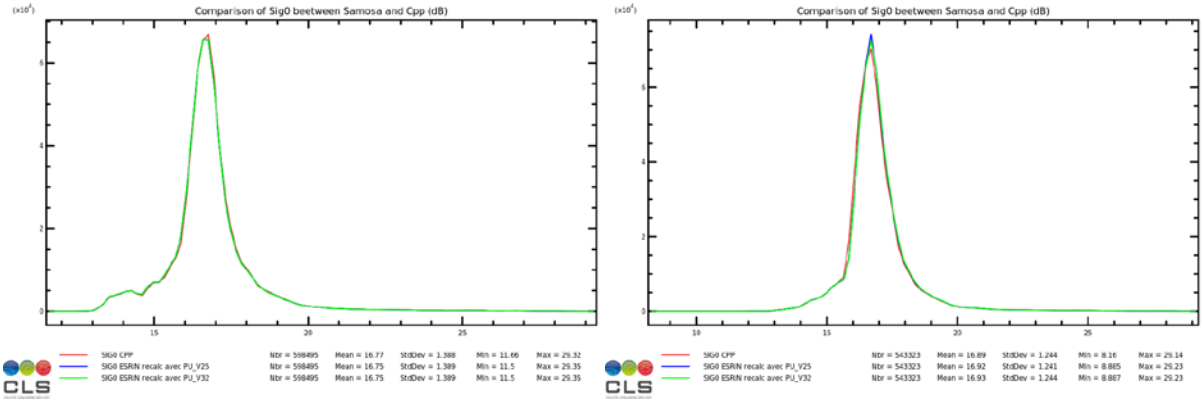

Figure 33: Histogram of 20-Hz Sigma0 from ESRIN SAR solution (in green and blue) and CPP (in red) in January 2013 for ascending (left panel) and descending (right panel) passes.

3.4.3. **Dependencies between parameters**

In Figure 34, the 20-Hz sigma0 residual is plotted as function of SWH. Their difference varies slightly with the wave height, and may be as high as ±0.1dB at 2m SWH. This result highlights a very good agreement between sigma0 estimates.

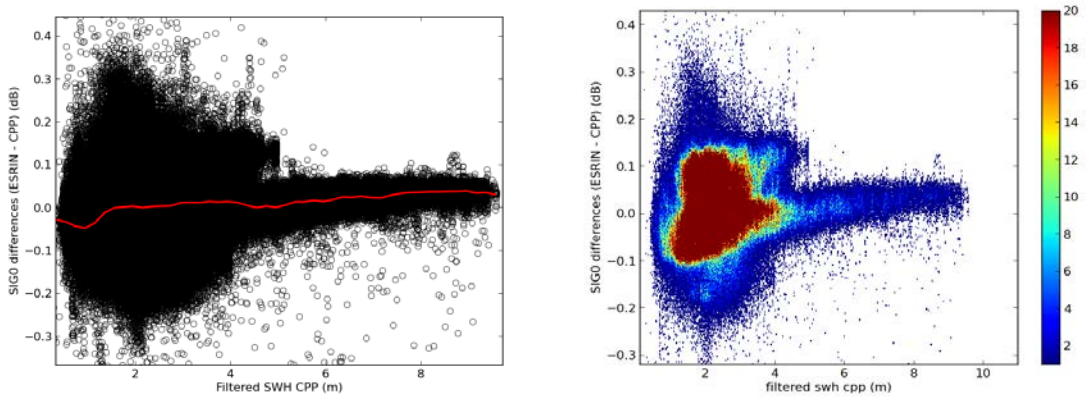

Figure 34: Dependencies of 20-Hz sigma0 residual with filtered SWH, in July 2012 and January 2013. Density of points in right panel.

Figure 35 and Figure 36 plot the same parameter as function of the radial velocity and mispointing angles (roll and pitch) respectively. In addition to the dependency to the wave height, the sigma0 residual appears to be also correlated to other parameters (roll angle and radial velocity notably and at a lesser extent pitch angle) that cannot be neglected.

It is however not clear to know which parameter is most correlated to the sigma0 residual. The radial velocity may impact the shape of the SAR echo waveform but the SAR retracking models are not taking account of this effect. We would thus expect to have similar impact on the estimates for both retrackers. In the other hand, the SAR retracking models which include the mispointing angles may exhibit some differences due to the way of taking account of this information. This issue would need further investigation extended to a much larger time period in order to draw more reliable conclusions.

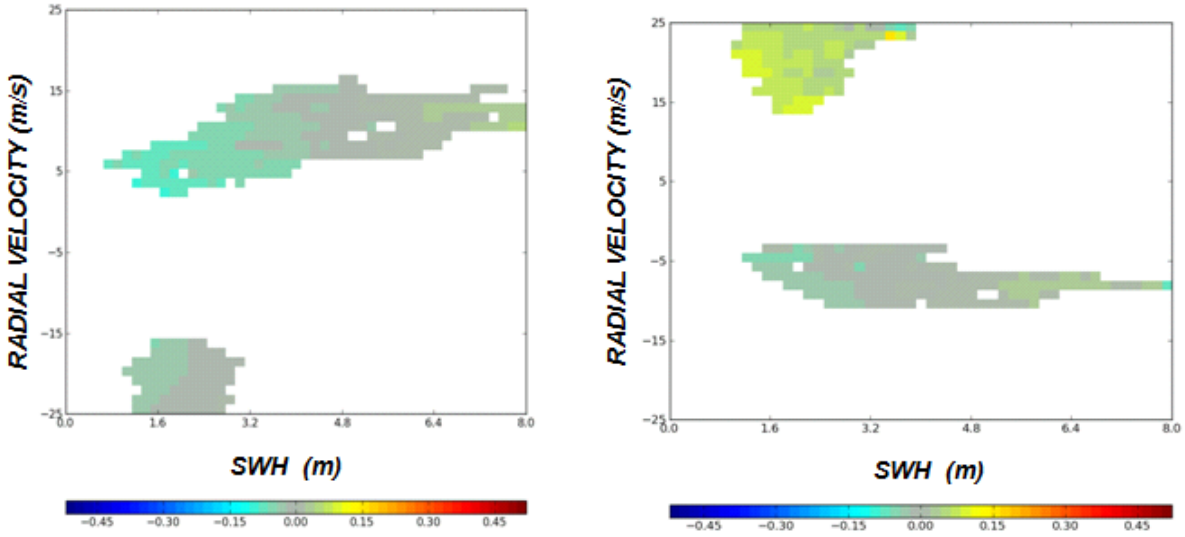

Figure 35: Dependencies of 20-Hz SIG0 residual (in dB unit) with filtered SWH and radial velocity in January 2013 for ascending (left panel) and descending (right panel) passes.

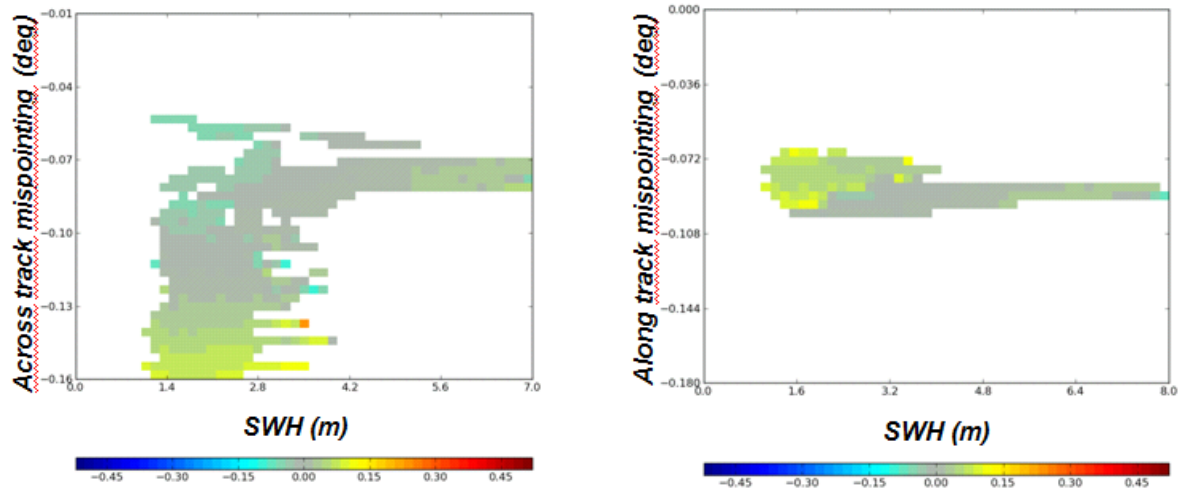

Figure 36: Dependencies of 20-Hz sigma0 residual (in dB unit) with across-track (left panel) and along-track (right panel) mispointing angles and filtered SWH in January 2013 for descending passes.

3.4.4. Sigma0 cartography

A map of differences between sigma0 computed by the ESRIN SAR solution and by the CPP retracker confirms the preceding results. The sigma0 residual plotted in Figure 37 (top panel) by 2°x2° geographical bins shows slight dependency with wave heights but stronger dependency on the across-track mispointing angle (for notably high roll angles) and possible correlation at a lesser extent with the radial velocity.

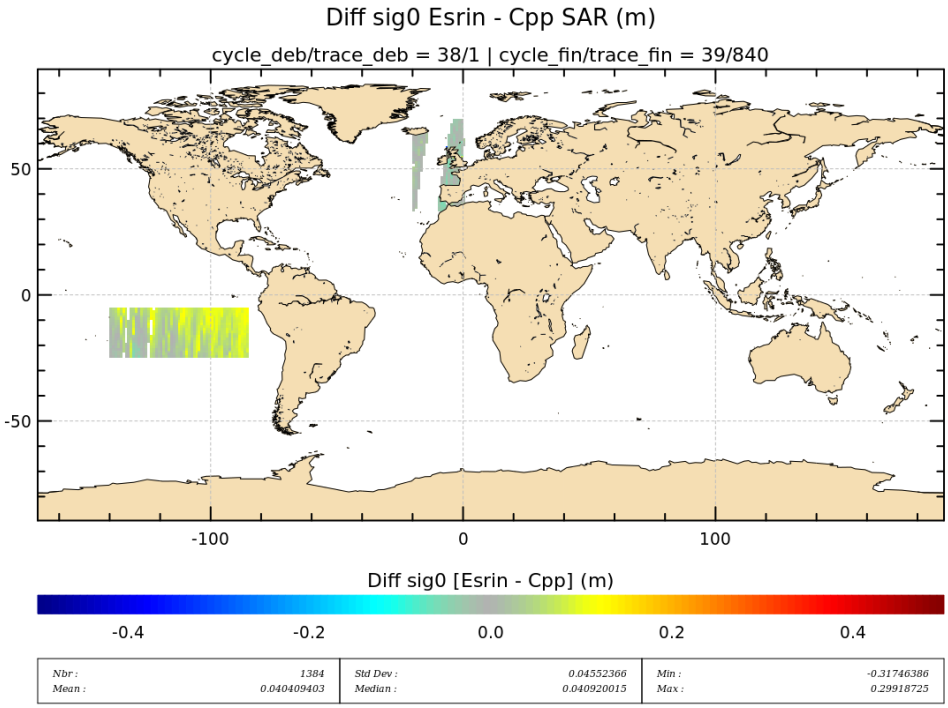
Diff sig0 Esrin - Cpp SAR (m)
cycle_deb/trace_deb = 38/1 | cycle_fin/trace_fin = 39/840
50
0
-50
-100
0
100
Diff sig0 [Esrin - Cpp] (m)
-0.4
-0.2
0.0
0.2
0.4
Nbr : 1384
Mean : 0.040409403
Std Dev : 0.04552366
Median : 0.040920015
Min : -0.31746386
Max : 0.29918725

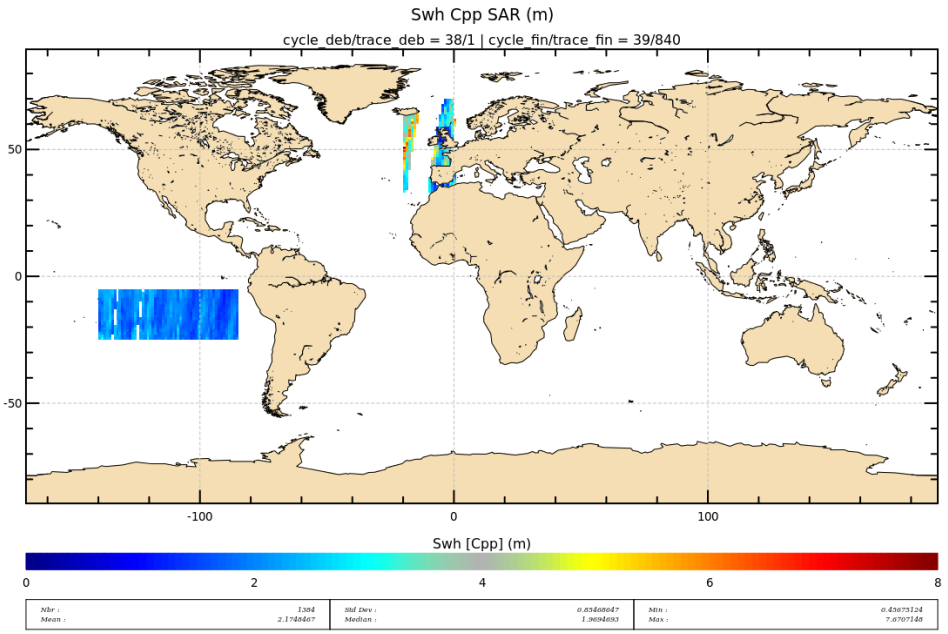
Swh Cpp SAR (m)
cycle_deb/trace_deb = 38/1 | cycle_fin/trace_fin = 39/840
50
0
-50
-100
0
100
Swh [Cpp] (m)
0
2
4
6
8
Nbr : 1304
Mean : 2.1748467
Std Dev : 0.8340647
Median : 1.9694693
Min : 0.4567124
Max : 7.6707148

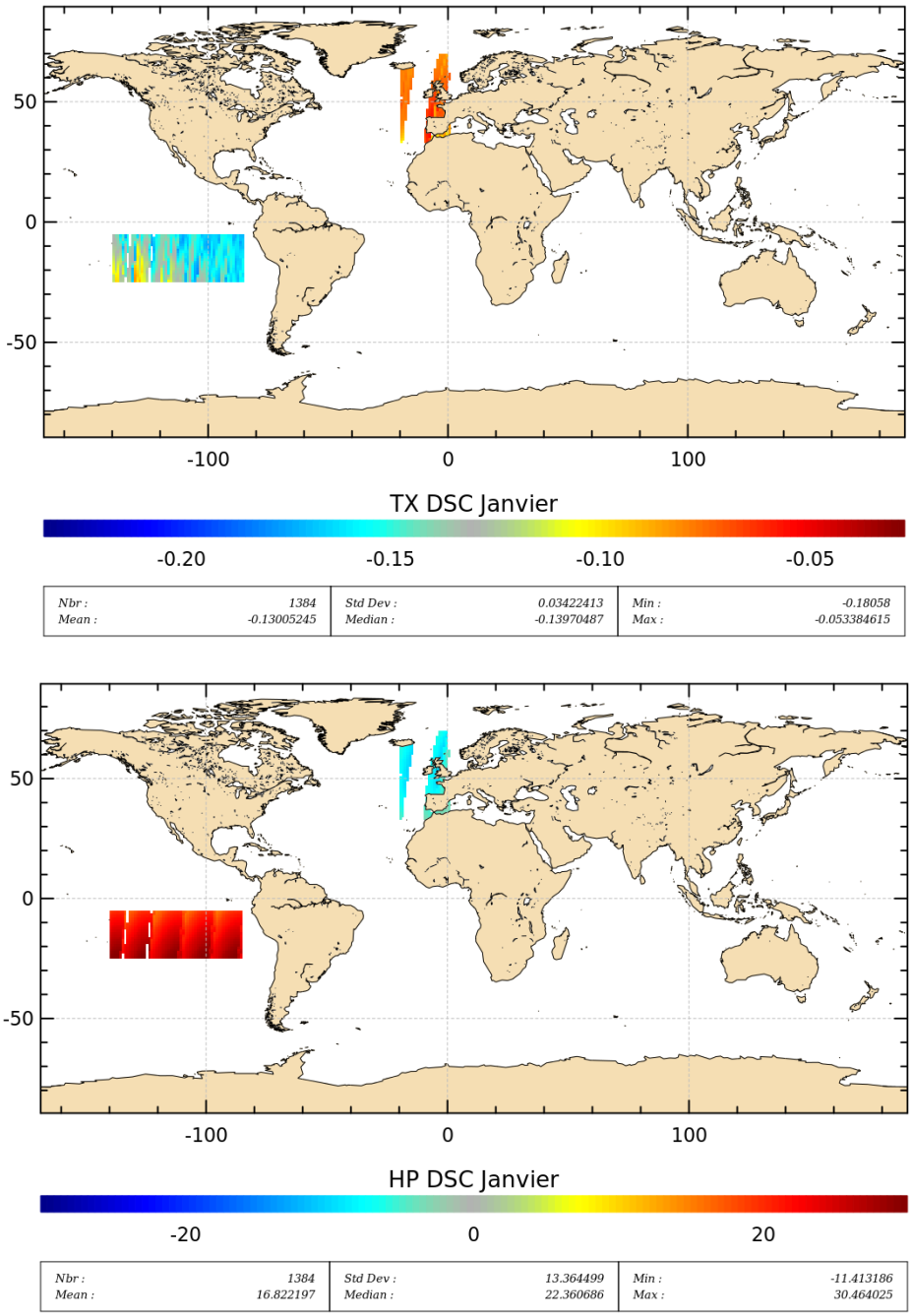

Figure 37: Difference of sigma0 from ESRIN SAR solution and CPP retrackers (top panel), and maps of different parameters in the following order: SWH, across-track mispointing angle and radial velocity, in January 2013 for descending passes.

3.4.5. **Comparison with RDSAR Sigma0**

In Figure 38 (top panel) one can observe that the SAR-mode sigma0 profile has apparent similarity with the RDSAR-mode, capturing same ocean structures. The SAR measurements are even likely to detect smaller scale structures (the heterogeneities within the LRM footprint) that are averaged and thus not seen by the RDSAR-mode measurements (for which sigma0 is like smoothed).

We smoothed the sigma0 retrieved from SAR-mode retracker (applying a 64 20-Hz points flat window function) to artificially make its footprint comparable to the RDSAR one (equivalent to a LRM radar footprint) and see whether the degraded SAR-mode sigma0 is consistent with the RDSAR-mode sigma0 or not. Figure 38 (bottom panel) shows a very good agreement between the smoothed SAR-mode sigma0 and the RDSAR one, ensuring that the accuracy and reliability of the SAR-mode retrieved backscatter coefficient are consistent with the LRM data

By analysing their differences plotted in Figure 39, we can notice that the RDSAR-mode and SAR-mode sigma0 are seemingly biased (as a first tentative, a rough calibration has been performed leading to an imprecise shift to both parameters with respect to the Jason-2 mission reference). The mean line of the 2D scatter plot (Figure 40) confirms this result. But the large cloud of points in the scatter plot also exhibits high differences that may be related to a drop of the SAR-mode sigma0 as it is observed in Figure 38 and Figure 39.

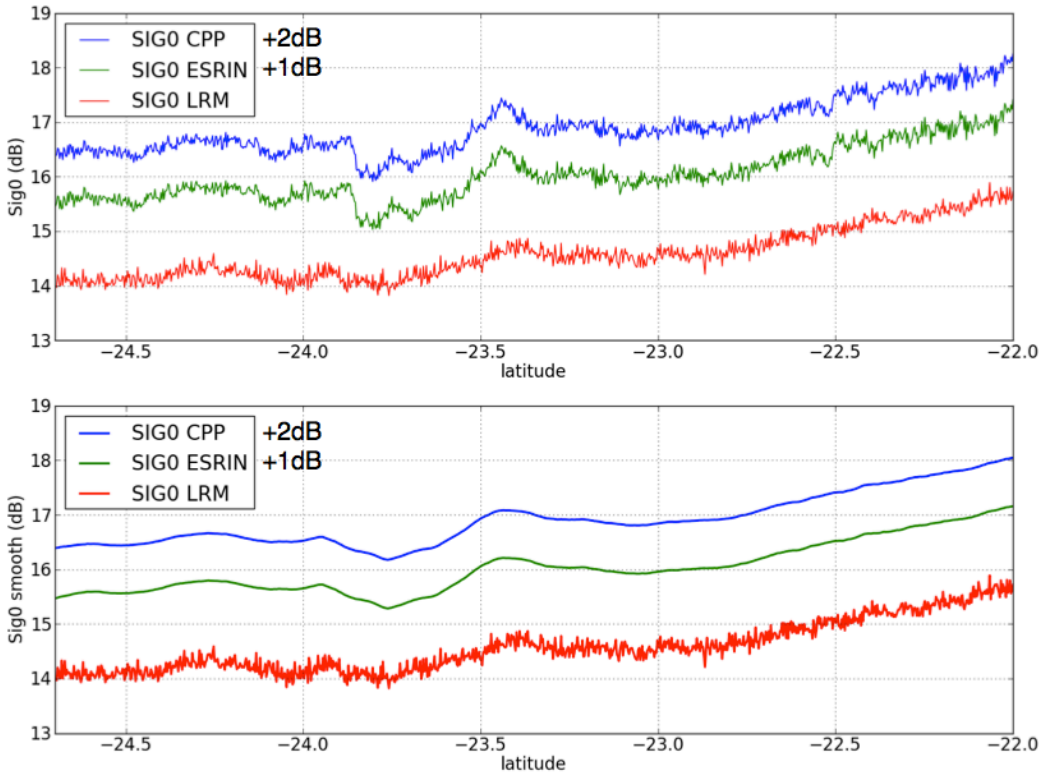

Figure 38: Along-track sigma0 (top panel) and smoothed SAR-mode sigma0 (bottom panel) as function as latitude. Sigma0 from CPP SAR retracker is in blue, sigma0 from ESRIN SAR solution retracker in green and RDSAR-mode sigma0 in red.

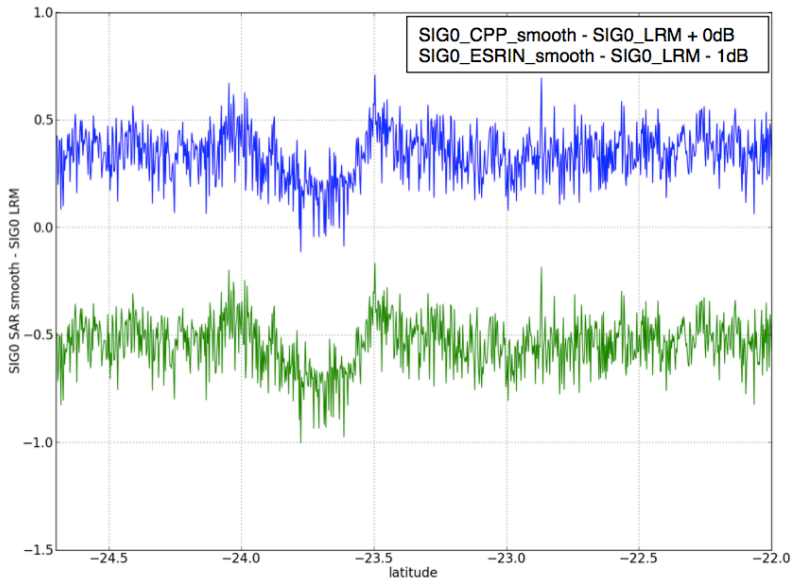

Figure 39: Along-track sigma0 difference as function of latitude. Residual between smoothed CPP SAR-mode sigma0 and RDSAR-mode sigma0 is in blue, and residual between smoothed ESRIN SAR-mode sigma0 and RDSAR-mode sigma0 in green.

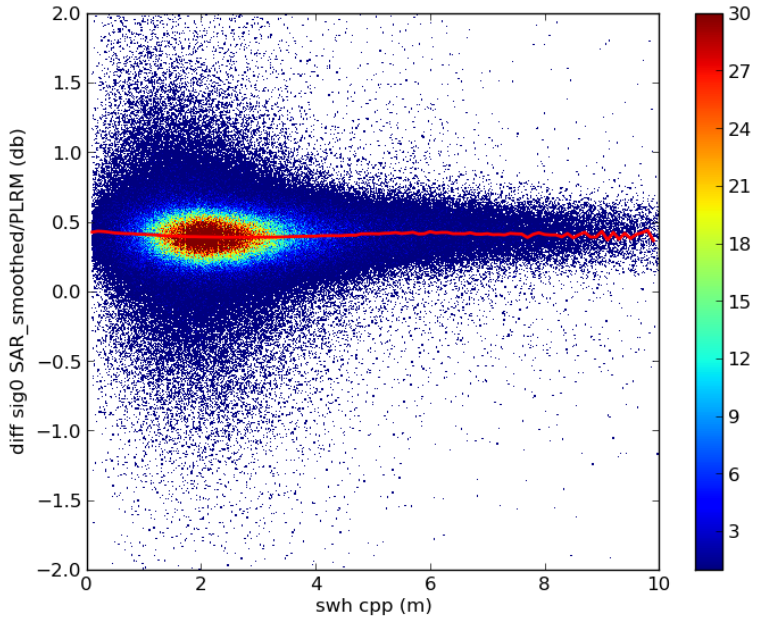

Figure 40: Difference between smoothed SAR-mode sigma0 and RDSAR-mode sigma0 as function of SWH, in July 2012 and January 2013. The red curve represents the mean of this difference.

4. Conclusion

Results of this study show that the agreement (for all parameters) between ESRIN SAR solution retracker outputs and CPP products is near perfect. Differences of few mm in range, few cm in wave height and one tenth of dB in sigma0 are reported, and are found to be primarily dependent on the significant waveheight, but also on roll angle (as seen in the sigma0 analysis) that have to be precisely evaluated.

However, all the observed differences are relatively small, and may be even considered as negligible. Thus, these results demonstrate that both retracking algorithms have very close behaviour and very similar performances. They are also well suited to derive very accurate and precise SAR altimeter measurements for the current CryoSat-2 mission and the coming Sentinel-3 one (and Jason-CS).

Also it should be emphasized that the assessment of the ESRIN SAR solution retracker has been performed with data from a restricted (two SAR-mode boxes), and over just a 2-month period of time, which may be critical. A larger set of data would most certainly be significantly more valuable for evaluating the quality of the promising ESRIN SAR solution retracker.

5. References

[Boy and Moreau, 2013]: F. Boy and T. Moreau, "*Algorithm Theoretical Basis Document (ATBD) of the CPP SAR numerical retracker for oceans",* CNES report, S3A-NT-SRAL-00099-CNES, June 15, 2013.

[Cotton and Martin-Puig, 2012]: D. Cotton and C. Martin-Puig, "*SAMOSA CCN D13 Final Project Report*", ESA contract report, February 6, 2012.

[Desjonquères et al., 2012]: J.D. Desjonquères, F. Boy and N. Picot, *"Altimeter SAR data over ocean – CNES processing strategy and continuity with LRM data"*, poster at the 2012 American Geophysical Union Meeting.

[Dinardo and Lucas, 2014]: S. Dinardo and B. Lucas, "SAMOSA *re-tracker configuration*", presented in CP4O meeting, Copenhagen, Denmark, March 25, 2014.

[Labroue et al., 2014]: S. Labroue, M. Raynal and T. Moreau, "*Validation report: WP5000 assessment of CPP SAR retracking*", CLS-DOS-NT-14-113, WP5000 CP4O report, May 20, 2014.

[Moreau et al., 2013]: T. Moreau, F.Boy and M. Raynal, "*Product Validation Report (PVR) of the CPP SAR numerical retracker for oceans*", CLS-DOS-NT-13-156, WP4000 CP4O report, June 24, 2013.